

Executive Summary

In response to climate change, caused by increasing pollution and further leading to deterioration of human health, future electricity generation should aim to reduce reliance on fossil fuels by increasing the use of renewable energy generation sources and also use clean vehicle technologies.

The objective of this project is to design and implement power converter topologies for bi-direction power flow in V2G (Vehicle to Grid) and G2V (Grid to Vehicle) technologies. It will support both the grid (in place) and traction (vehicle) with added auxiliary loads, Also by controlling bidirectional charging and discharging services of battery efficiently, it can further make it more suitable for renewable energy integration. A better solution where the battery system can be used to support the services, wherein the battery is still part of the source.

This can improve supply grid efficiency, reliability, stability, and generation dispatch if it is designed, controlled and implemented in a smart grid by properly handling critical issues such as, the greater numbers of EVs connected causing disruption to existing energy grid.

Thus this project will provide a detailed technical assessment, with various power electronics topologies, modeling and control strategies designed in terms of harmonics and dynamic response.

	CONTENTS	Page No.
Acknowledgements		i
Executive Summary		ii
Table of Contents		iii
List of Figures		vii
List of Tables		viii
List of Abbreviations		ix
1 INTRODUCTION AND GOALS OF THE PROJECT		1
1.1 Motivation		2
1.2 Objective		2
1.3 Background		3
1.3.1 Conductive and Inductive Chargers		3
1.3.2 On-Board and Off-Board Chargers		4
1.3.3 Unidirectional and Bidirectional Chargers		5
2 PROPOSED WORK		6
2.1 V2G and G2V Configuration		6
2.2 Common Charging Methods		7
2.2.1 Constant Voltage Charging		7
2.2.2 Constant Current Charging		7
2.2.3 Combined Charging		7
3 IMPLEMENTATION OF TOPOLOGIES		9
3.1 Three Phase Full Bridge Converter		9
3.1.1 Mathematical Modeling		11
3.1.2 Modeling Parameters		12
3.1.3 Three Phase Full Bridge Converter Results		12

3.2	Three Phase PWM Inverter	13
3.2.1	Modeling Parameters	13
3.2.2	Three Phase PWM Inverter Results	14
3.3	Switching Regulation	16
3.4	Boost Converter	16
3.4.1	Design of Capacitor	17
3.4.2	Design of Inductor	17
3.5	Buck Converter	18
3.5.1	Design of Inductor	18
3.5.2	Design of Capacitor	18
3.6	DC-DC converter for LDV	19
3.6.1	Modeling Parameters	20
3.6.2	DC-DC Converter for LDV Results	21
3.7	Full Bridge Two-Quad Converter for HDV	22
3.7.1	Modeling Parameters	23
3.7.2	Full Bridge Two-quad Converter for HDV Results	24
3.8	Implementing Reverse charging	24
3.8.1	Modeling Parameters	25
3.8.2	Implementing Reverse Charging Results	26
4	DESIGN OF SUBSYSTEMS AND CONTROLLER	28
4.1	On-board / Off-board Subsystems	28
4.1.1	Three phase Bidirectional AC/DC Converter Subsystem	28
4.1.2	DC/DC Converter Switches Subsystem	29
4.2	Phase-Locked-Loop (PLL) Controller	30
4.2.1	PLL - Voltage Controller	30
4.2.2	PLL - Current Controller	31

4.2.3	Power Flow using PLL Controller	33
4.2.4	Battery Charging and Discharging Controller	35
5	IMPLEMENTING AUTONOMOUS V2G-G2V CONTROLLED OPERATION	38
5.1	V2G-G2V Operation Controlled with a Toggle Switch	38
5.1.1	Modeling Parameters	39
5.1.2	Working Operations	39
5.1.3	V2G Results	40
5.1.4	G2V Results	41
5.1.5	Abrupt Change In Operations Results	43
5.2	V2G-G2V with Parallel Operation of Batteries	45
5.2.1	Modeling Parameters	45
5.2.2	V2G With Parallel Operation Results	46
5.2.3	G2V With Parallel Operation Results	47
5.3	THD Comparison	48
5.3.1	THD in Single Battery V2G-G2V Operation	48
5.3.2	THD in Parallel Operation of Batteries V2G-G2V Operation	49
6	CONCLUSION AND POSSIBLE FUTURE WORK	50
6.1	Performance Related to Operations	50
6.2	Results	51
6.3	Conclusion	51
6.4	Future Work	51
References		52
Curriculum Vitae		54
Capstone Project Summary		55

List of Figures

Figure No.	Title	Page No.
1.3.3	Power flow in a general charger's structure	5
3.1.1	Circuit diagram of three phase fully controlled full wave bridge converter	9
3.1.2	Three phase full wave bridge converter with $\alpha=90^\circ$	12
3.2.1	Three Phase PWM Inverter	13
3.2.2a	Input to 3-phase PWM Inverter	14
3.2.2b	Output Phase-Voltage of three phase Inverter	14
3.2.2c	Output Line voltage of three phase Inverter	15
3.6.1	Two- quad (full bridge) converter for (LDV)	19
3.6.2a	Charging Output	21
3.6.2b	Discharging Output	21
3.7.1	Circuit for full bridge two-Quadrant converter for Heavy-Duty Vehicles (HDV)	22
3.7.2	Charging Output	24
3.8.1	Implementation of V2G	24
3.8.2a	Battery status after implementing V2G	26
3.8.2b	Output phase with Resistive load without Filter voltage of V2G	26
3.8.2c	Output phase voltage with LCL filter of V2G	27
4.1.1	AC/DC Converter Subsystem	28
4.1.2	DC/DC converter subsystem	29
4.2.1a	V_{abc} converting into V_{dq0} frame	30
4.2.1b	PLL closed loop	31
4.2.2a	I_{RYB} converted to I_{dq0}	31
4.2.2b	PLL current controller	32
4.2.3a	Active current flow phasor diagram	33

4.2.3b	Phasor diagram for lagging reactive current transfer	33
4.2.3c	Phasor diagram for leading reactive current transfer	34
4.2.4a	Battery charging controller	35
4.2.4b	Battery controller responses in V2G operation	36
4.2.4c	Battery controller responses in G2V operation	36
4.2.4d	Battery controller responses at abrupt change of operation from V2G to G2V	37
5.1.1	Simulink model for V2G-G2V operation controlled via a toggle switch	38
5.1.3a	Battery performance in V2G mode	40
5.1.3b	Three phase grid voltages and current in V2G mode	40
5.1.3c	DC link voltage in V2G mode	41
5.1.4a	Battery performance in G2V mode	41
5.1.4b	Three phase grid voltages and current in G2V mode	42
5.1.4c	DC link voltage in G2V mode	42
5.1.5a	Battery performance when V2G is changed to G2V mode	43
5.1.5b	Three phase grid voltages and current at change of operating mode	43
5.1.5c	DC link voltage at change of operating mode	44
5.2.1	Simulink model for V2G-G2V topology with parallel operation of battery	44
5.2.2a	Three phase grid voltages and current in V2G mode with parallel operation of batteries	46
5.2.2b	DC-link voltage in V2G mode with parallel operation of batteries	46
5.2.3a	Three phase grid voltages and current in G2V mode with parallel operation of batteries	47
5.2.3b	DC-link voltage in G2V mode with parallel operation of batteries	47
5.3.1	FFT window of single battery V2G-G2V operation	48
5.3.2	FFT window of parallel battery V2G-G2V operation	49

List of Tables

Table No.	Title	Page No.
1.3.1	Comparison between conductive and inductive charges	3
1.3.2	Comparison between On-Board and Off-Board chargers	4
1.3.3	Comparison between unidirectional and bidirectional chargers	5
2.2.3	Comparison-of-different-charging-modes	8
3.1.1	Different Modes of Operation	11
3.1.2	Modeling parameters for three phase full bridge converter	12
3.2.1	Modeling parameters for three phase PWM inverter	13
3.6.1	Modeling parameters for DC/DC converters	20
3.7.1	Modeling parameters for two- quad HDV converter	23
3.8.1	Modeling parameters for reverse charging	25
4.2.3	Condition for flow of grid current	34
5.1.1	Modeling parameters for automated V2G-G2V topology	39
5.2.1	Modeling parameters for V2G-G2V with parallel operation of batteries	45
6.1	Performance parameters of V2G and G2V mode at t=0.505 sec	50

List of Abbreviations

EV	Electric vehicle
G2V	Grid-to-vehicle
V2G	Vehicle-to-grid
PEVs	Plug-in electric vehicles
PHEVs	Plug-in hybrid vehicles
OCV	Open Circuit Voltage
SoC	State-of-Charge (%)
AC	Alternating Current
DC	Direct Current
CC	Constant current
CV	Constant voltage
PLL	Phase locked loop
HV	High voltage
EMC	Electromagnetic compatibility
LV	Low voltage
HV	High Voltage
LDV	Low Duty Vehicle
HDV	Heavy Duty Vehicle
MOSFET	Metal-oxide-semiconductor field-effect transistor
IGBT	Insulated-gate bipolar transistor
GTO	Gate Turn-Off Switch
THD	Total harmonic distortion
FFT	Fast Fourier transform

1. INTRODUCTION AND GOALS OF THE PROJECT

The V2G/G2V transfer power/energy from vehicle to the grid and vice-versa for many applications which can improve grid efficiency and stability if it is properly controlled and implemented in a smart grid, further increasing reliability to integrate various other loads . It can also provide auxiliary services, including power factor improvement, harmonics reduction, and storage system support.

In Spite of its advantages, the V2G application is evolving, being in its early stages. Manufacturers should take care that the vehicle is charged and has suitable conditions when it is required in order to connect and spread the use. At the same time, it is critical that the V2G application does not disrupt the energy grid. To meet this constraint, a power factor correction system must be used, harmonics must be reduced (while maintaining EMC regulations), and DC currents must be eliminated in order to not saturate the grid's transformers. A proper phase lock has to be maintained to synchronize and balance the load conditions.

This system also has to be manufactured by keeping a view for future needs for auxiliary services, this may involve an integration with a house, an EV, or any private power systems.

The degradation of the battery should also be addressed, since an increase in charge-discharge cycles might shorten its life. Moreover, the greater the number of EVs connected to the grid, the more serious the preceding power distribution system issues become. The major goal of this work is demonstrating how different V2G - G2V topologies may be implemented using Matlab/Simulink.

1.1 MOTIVATION

Today because of energy dependence on fossil fuels, which has caused major concerns related to climate change and pollution, Our major aim should be in the use of renewable energies, in which a crucial role is played by electrification of transportation systems. Addressing an issue of variability inherent in renewable energies by use of energy storage systems, where EVs can play an advantageous role over other traditional energy storage systems. EVs have many advantages such as easy implementation, environment friendly, and it carries an on-board storage system which can be used for implementation of V2G and G2V technologies. These EVs are categorized in three groups such as, light duty, medium duty and heavy duty depending on usage and requirements for example passengers cars, vans and bus respectively.

1.2 OBJECTIVE

Energy storage systems are critical grid components because they allow irregular renewable energy sources to be integrated. When electric vehicle (EV) batteries are hooked in for charging, it can effectively be used as equivalent to storage devices in the grid. It is observed that the majority of personal EVs (cars) are parked on an average for around 22 hours each day, during this time it being an idle asset. EVs have the inherent ability to aid grid energy by storing energy when there is an excess with the help of G2V and providing/injecting the energy back to the grid as and when required with V2G. V2G implementation has to tackle some obstacles, facing difficulty to control abnormal operations, requiring a significant number of EVs to meet grid requirements, and being difficult to implement in the short term. It is simple to create a V2G system in this scenario.

The main objective is to design and control converters for bidirectional operations (single phase and three phase), which is used for its easy implementation by allowing a transformerless system to simulate different topologies and with parallel operation of batteries i.e multiple EVs connected in parallel.

The converters and their controls will be designed and simulated using Matlab/Simulink. This will provide an overview of the various converter topologies in power

electronics, modeling and control approaches devised in terms of dynamic response and harmonics. As long as proper supervision is in place, this technology can give various benefits to the electrical grid. It gives a way for controlling the amount of energy delivered or taken from the battery through effective charging and discharging. Also, the grid current is used to establish a current control loop (PLL-controller) for the converter switching patterns and to control the energy flow.

1.3 BACKGROUND OF CHARGERS

This section will give a general overview of different types of charger.

1.3.1 CONDUCTIVE CHARGERS AND INDUCTIVE CHARGERS

EVs and grid connection can be conductive (wired) or inductive (wireless). In wired charger i.e conductive charger EV uses a cable which is manually plugged in by the user, though there exist some safety risks in rain/wet conditions and automation cannot be implemented. On the other hand wireless i.e inductive charger is connected magnetically this consist of two components, the AC grid current is taken to (on-board/off-board) AC/DC converter rectifying it to connected to the battery, At each end, a winding is placed forming a transformer through which the power is transmitted, making an electrical isolation.

The advantages and disadvantages of these chargers are compared in table 1.3.1.

Table 1.3.1: Comparison between conductive and inductive chargers

Type	Advantages	Disadvantages
Conductive	Both slow and fast charging Easy implementation More Efficient	Plug-in (manually) Risks in rain/wet conditions Challenge for automation
Inductive	Easy for user Weather proof More safer Conductive isolation Easier automation	Lower efficiency Slow charging Loss power density High complexity in manufacturing Non exchangeability (design specific)

1.3.2 ON-BOARD AND OFF-BOARD CHARGERS

The charger subsystem included in the vehicle or not, respectively makes it On-board and Off-board chargers. Owing to the constraints such as cost, weight and space requirement for on-board charger are limited to slow charging, but their major advantage is its capability to work with any suitable power outlets for example household, increasing its acceptance hugely. Use On-board configuration charger infrastructure is majorly at home during night and this has minimal impact on grid supply and can help in control of load level which is usually less in demand at night.

Off-Board chargers have capability to work much faster compared to on-board ones because they do not have constraints for space or weight, further it takes power from the grid to battery (EVs) by converting it to DC. Off-Board charge cuts extra power electronics circuits and cost of EVs. A concise comparison between on/off- board chargers is given in table 1.3.2.

Table 1.3.2: Comparison between On-Board and Off-Board chargers

Type	Advantages	Disadvantages
On-board	Lower price Compact in size High availability of charging Minimal grid impact	Slow charging Power limitation Weight and size constraints
Off-board	Faster charging No constraints on size or weight Enables long distance traveling	Higher price More impact to grid Slow development of charging infrastructure

1.3.3 UNIDIRECTIONAL AND BIDIRECTIONAL CHARGERS

A charger comprises power electronics circuits that are used for different applications that convert electrical energy from various power sources. Converters are designed as per the requirement power requirement or flow between the grid and the battery, so this charging and discharging requirements are classified as unidirectional and bidirectional power flow, a basic charger's structure is shown in below Fig 1.3.3.

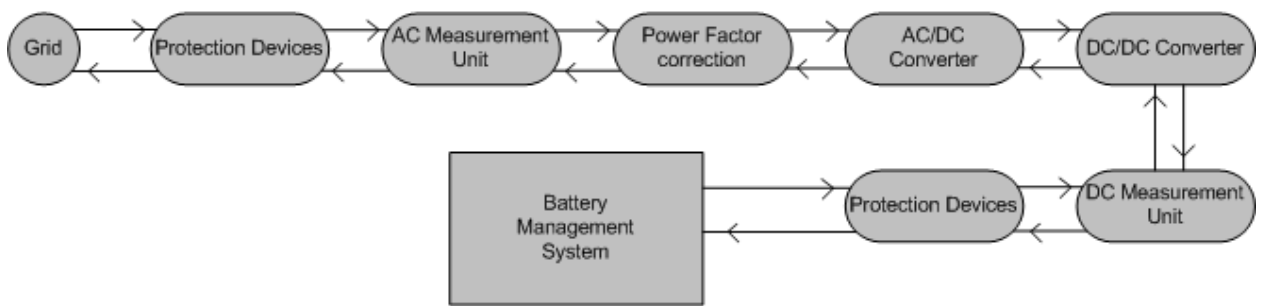


Figure 1.3.3: Power flow in a charger

The unidirectional chargers are simple, require less hardware and cause less battery degradation, typically consisting of a rectifier, a filter (L, LC or LCL), and a DC-to-DC converter, but being unidirectional V2G - G2V applications are limited. Contrary, bidirectional chargers are more complex and can provide great grid and EV connectivity with higher quality of support for auxiliary loads. This typically consists of two stages, a bidirectional AC-to-DC converter for the grid connection and a bidirectional DC-to-DC converter for the battery connection. An insight between unidirectional and bidirectional chargers is given in table 1.3.3.

Table 1.3.3: Comparison between unidirectional and bidirectional chargers

Unidirectional	Bidirectional
Simple control Less hardware Safer Less battery degradation Lower Efficiency	Complex Control More hardware and information exchange required Need of safety measures, anti-islanding protection Degradation due to frequent cycling High Efficiency

2. PROPOSED WORK

EV's charger can be categorized and designed for different topologies and usage depending on the battery pack's voltage.

1. High-Voltage Batteries

With HV (Heavy-Voltage) battery pack only single-phase bidirectional structures, an AC-to-DC converter is used for grid connections, though it could be switched to a three phase model for higher power applications.

2. Low-Voltage Batteries

LV (Low-Voltage) batteries require an intermediate DC/DC converter to increase i.e to boost the battery voltage to match the required value in the DC-link bus in addition to AC/DC converter which is further connected to the grid.

2.1 V2G AND G2V CONFIGURATION

Matlab-Simulink is used to design and simulate bidirectional single-phase and 3-phase V2G and G2V system chargers with Lithium-ion batteries which are the most common battery technologies utilized in electric vehicles.

A three phase fully controlled full wave rectifier bridge rectifier, three phase PWM inverter, DC/DC converter for LDV and full bridge two-quadrant converter (G2V) and with reverse charging (V2G) are some basic topologies simulated to implement the technology.

To regulate the amount of energy flow i.e taken or delivered to the battery, a charging and discharging PLL-control strategy is established, by creating the grid current reference for an internal closed control loop to produce switching pattern for the converter switches. PLL is used to synchronize the reference current to the grid voltage.

2.2 COMMON CHARGING METHODS

This sanction provides a brief description of common charging methods which are explained below

2.2.1 CONSTANT VOLTAGE CHARGING (CV)

In this method the complete charging process current is not-limited i.e unconstrained and the highest value of voltage is used. Current begins with high value and it decreases gradually as the battery gets charged.

2.2.2 CONSTANT CURRENT CHARGING (CC)

The voltage increases as the battery charges while the current applied remains constant. If the battery spent really charges until its impedance is not zero.

2.2.3 COMBINED CHARGING (CC-CV)

This method allows a complete charge without getting overcharged so the combined charging CC-CV method is the most preferred for lithium (Li-ion) batteries. It starts with CC charging till voltage reaches its maximum value, once the maximum value is obtained CV charging begins with current decreasing till battery gets fully charged maintaining voltage at its highest value.

Comparison between different types of charging modes is given in below table 2.2.3.

Table 2.2.3: Comparison-of-different-charging-modes

Method	Advantages	Disadvantages	Key Parameters
Constant Voltage (CV)	Easy implementation	Can cause battery lattice to collapse	voltage charging rate
Constant Current (CC)	Easy implementation	Low Capacity utilization	current charging rate
Constant Current-Constant Voltage (CC-CV)	High Capacity utilization Stable terminal voltage	Challenge is to balance speed, energy loss, temperature while charging.	Charging current in CC mode Charging voltage in CV mode

3. IMPLEMENTATION OF TOPOLOGIES

This chapter will deal with several different topologies used for charging and discharging model implemented for V2G and G2V technologies

3.1 THREE PHASE FULL BRIDGE CONVERTER

Three-phase controlled full wave bridge-converter which is also known as a 6-pulse converter. It is used to rectify AC with 6 thyristor in bridge connection, as shown in Fig 3.1.1.

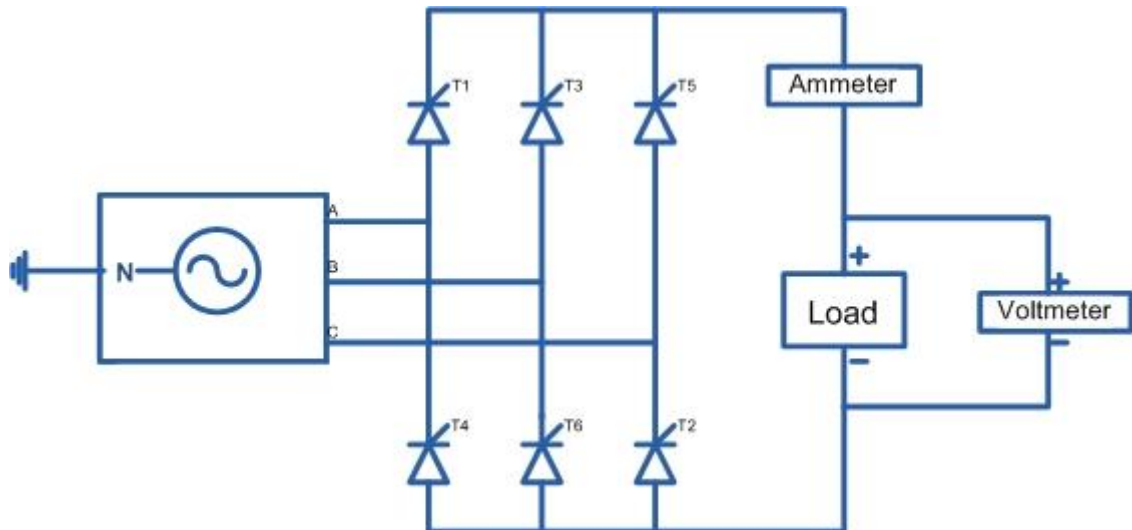


Figure 3.1.1: Circuit diagram of three phase fully controlled full wave bridge converter

When a thyristor is formed by connecting two three-pulse midpoint converters in series or parallel, the conduction time of the thyristor in a six-pulse connection can be extended. Figure 3.1.1 depicts the converter arrangement. The positive group is the three-pulse converter that feeds current to the load, while the negative group is the one that provides the current return path. When compared to a three-pulse converter, there are some advantages:

1. The mean output voltage is double that of a three-pulse converter for the same source because the converters are connected in series on the dc side.
2. The number of pulses is raised to six, while the ac ripple amplitude is reduced.
3. The dc component in the transformer's secondary is fully removed. If this feature is used, the transformer's design rating is reduced. Because the transformer windings convey current in both directions, bridge connections are referred to as two-way circuits. This helps in core's dc magnetization elimination. Midpoint connections, on the other hand, lack this feature and are thus one-way connections. When compared to a Six pulse bridge converter, the bridge connection has thyristors conducting for 120° , which increases the use of both the thyristors and the transformer. The algebraic sum of the component converters' voltages is the bridge converter's output voltage.
4. Two thyristors conduct at all times, one from the positive(T1,T3,T5) and the other from the negative(T4,T6,T2) group of thyristor. The firing angle can be adjusted between 0 and 180 degrees. The natural firing moment is specified by the firing angle $\alpha = 0$, which has already been defined in the case of a three-pulse converter. The average dc voltage drops to zero as the firing angle approaches 90 degrees. The converter is in the rectifying mode and power is flowing from ac to dc.

3.1.1 MATHEMATICAL MODELING

The output average load voltage of this 6-pulse converter i.e voltage pulses is given by

$$V_{odc} = \frac{3\sqrt{3}}{\pi} V_m \cos \alpha \quad (3.1)$$

Here, peak line voltage: $V_{mL} = \sqrt{3} V_m$. (3.2)

$$\text{Gives } V_{dc(max)} = V_{dm} = \frac{3\sqrt{3}Vm}{\pi} = \frac{3VmL}{\pi} \quad (3.3)$$

$$\text{The average dc output voltage is normalized as } V_{dcn} = V_n = \frac{Vdc}{Vdm} = \cos \alpha \quad (3.4)$$

$$\text{The output voltage's rms value is calculated using } V_{orms} = \sqrt{3} V_m \left(\frac{1}{2} + \frac{3\sqrt{3}}{4\pi} \cos 2\alpha \right)^{1/2} \quad (3.5)$$

Different Modes of Operation with respect to firing angle alpha to all switches i.e thyristors and their respective conducting pairs are shown in Table 3.1.1.

Table 3.1.1 Different Modes of Operation

Mode	ωt	Incoming SCR	Outgoing SCR	Conducting Pair	Load voltage
1	$30+\alpha$	T1	T5	T6, T1	V_{ab}
2	$90+\alpha$	T2	T6	T1, T2	V_{ac}
3	$150+\alpha$	T3	T1	T2, T3	V_{bc}
4	$210+\alpha$	T4	T2	T3, T4	V_{ba}
5	$270+\alpha$	T5	T3	T4, T5	V_{ca}
6	$330+\alpha$	T6	T4	T5, T6	V_{cb}

3.1.2 MODELING PARAMETERS

Following table 3.1.2 represents the parameters used in simulation of the three phase fully controlled full wave bridge converter.

Table 3.1.2: Modeling parameters for three phase full bridge converter

Circuit Element	Parameter	Values
Pulse generator (T1):	Amplitude	1
	Period	0.02 sec
	Pulse width	10
	Phase delay	(1.667e-3)*4 i.e ($\alpha = 90^\circ$)
3-Φ Supply:	V_{line} (rms)	415
	Frequency	50Hz
Resistive (Load):	Resistance	10 ohms

3.1.3 THREE PHASE FULL BRIDGE CONVERTER RESULTS

Result waveform in Fig 3.1.2, of a three phase full wave bridge converter with firing angle to T1 is $\alpha=90^\circ$, shows input 3 phase voltages, first pulse generator waveform, Output voltage and output current.

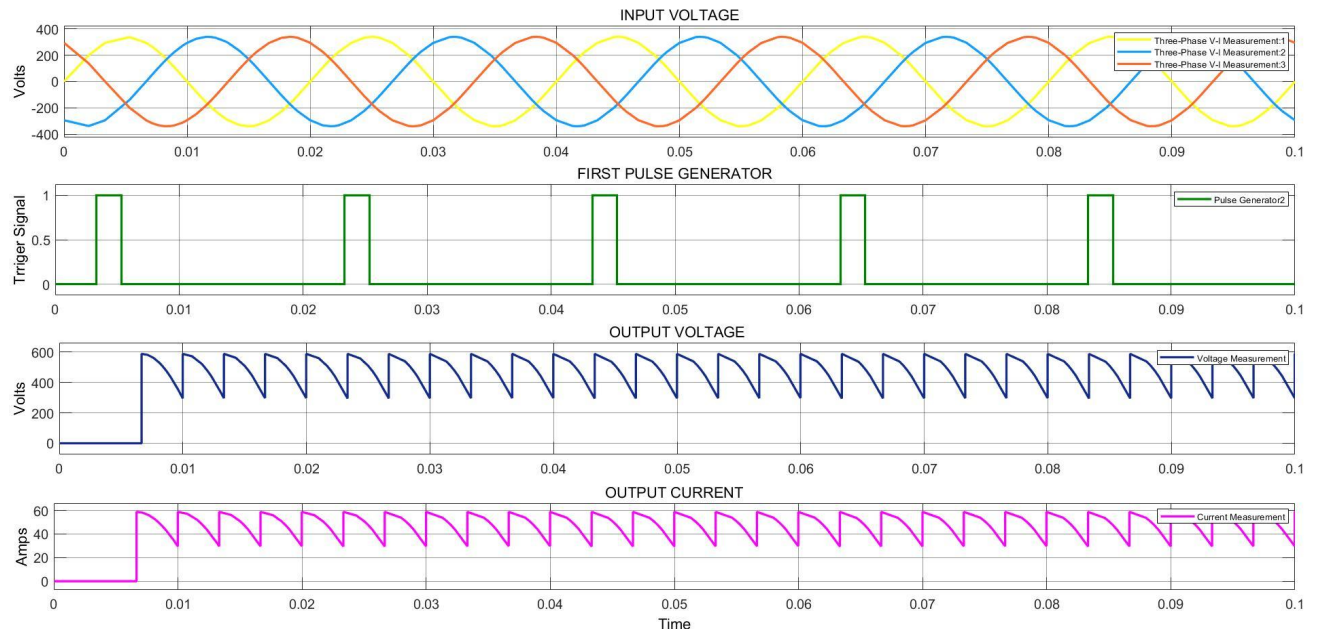


Figure 3.1.2: Three phase full wave bridge converter with $\alpha=90^\circ$

3.2 THREE PHASE PWM INVERTER

Three Phase sine pulse width modulation bridge inverter i.e inverting controlled with signal generated by DC with sin and sawtooth comparison, which is fed to the switches, as demonstrated in Fig 3.2.1.

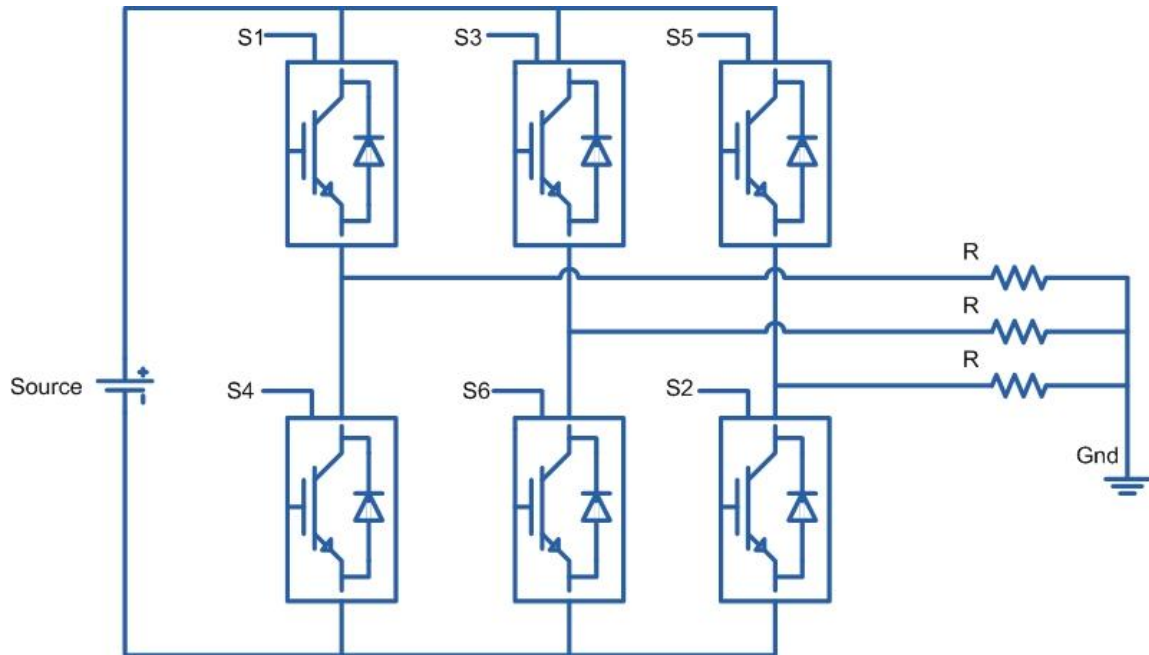


Figure. 3.2.1: Three Phase PWM Inverter

3.2.1 MODELING PARAMETERS

Following table 3.2.1 represents the parameters used in modeling of sine- PWM inverter (three phase).

Table 3.2.1: Modeling parameters for three phase PWM inverter

Circuit Element	Parameter	Values
Sine wave:	Amplitude	1
	Frequency	$2\pi \times 50$ (rad/sec)
3-Φ Sawtooth Generator	Frequency	1e3 Hz
	Phase Angle	180°
Resistive (Load):	Resistance	10 ohms
DC source	Voltage	100 V

3.2.2 THREE PHASE PWM INVERTER RESULTS

Result waveform in Figure 3.2.2a, of three phase sine-PWM bridge inverter, shows controlling of PWM input i.e by logical comparison of sine wave and sawtooth wave, further output phase and line voltages of three phases in Fig 3.2.2b and 3.2.2c respectively.

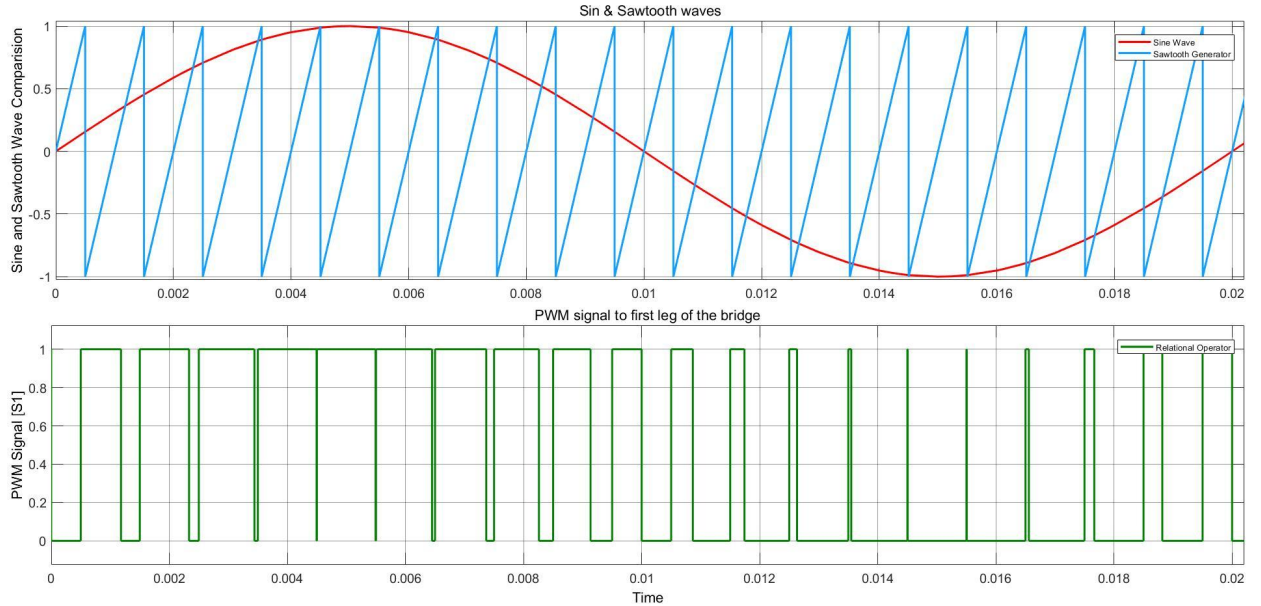


Figure 3.2.2a: Input to 3-phase PWM Inverter

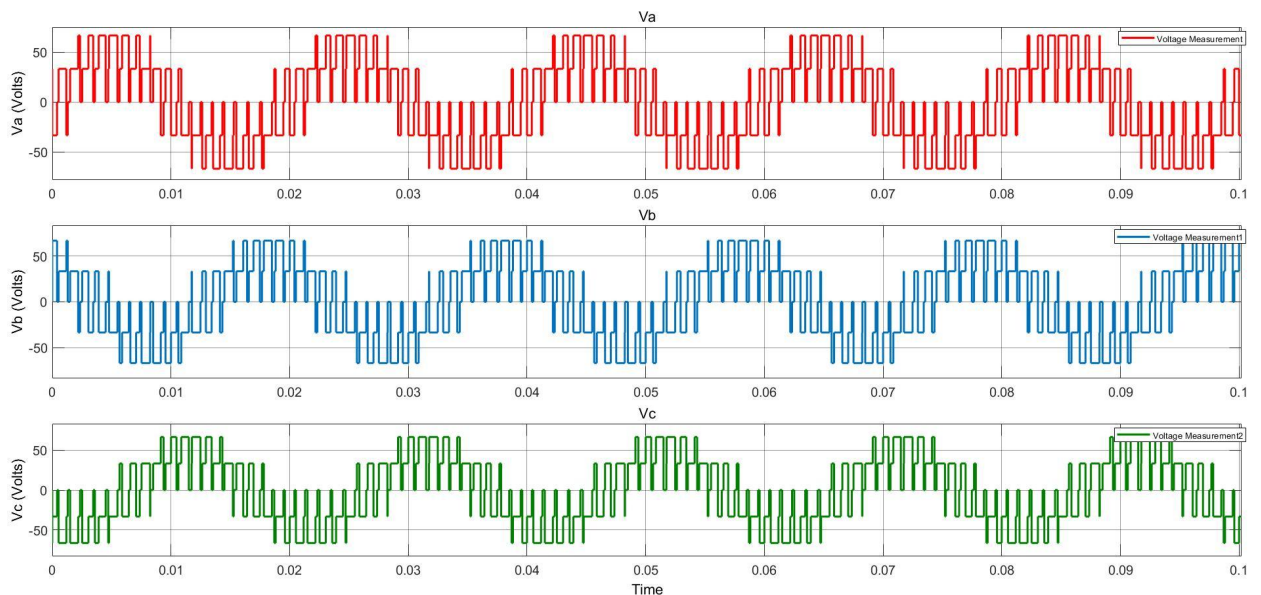


Figure 3.2.2b: Output Phase-Voltage of three phase Inverter

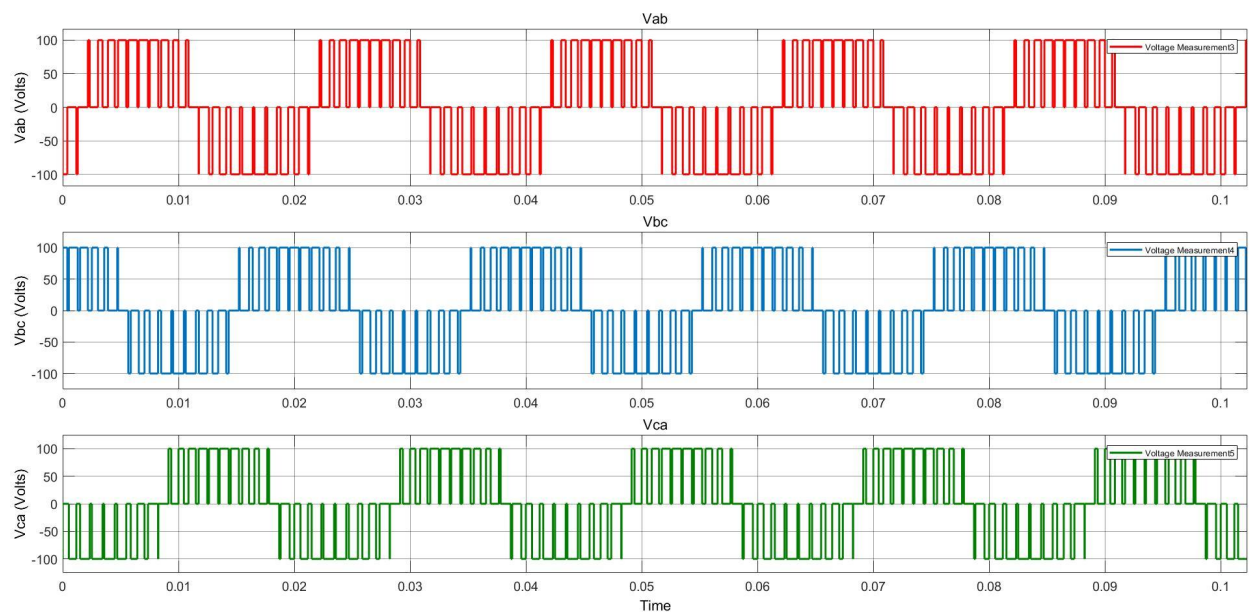


Figure 3.2.2c: Output Line voltage of three phase Inverter

3.3 SWITCHING REGULATION

Switching power supply can step up and step down voltages efficiently and can also provide isolation between output and input voltages. The inductor used to limit slew rate and store energy. This energy is a function of current i.e $E = \frac{1}{2} \times L \times I^2$ (3.6)

A switch regulator consists of a diode, a power switch and an inductor for transfer of energy. The rearrangement of components can form step-up (boost) converter or step-down (buck) converter. To maintain constant output and to regulate energy transfer, a control and feedback circuitry is placed.

3.4 BOOST CONVERTER

A boost converter is a step up DC-to-DC converter consisting of two power semiconductors and energy storage elements like capacitor and inductor that step-up the input voltage.

Essentially it is a combination of step-up chopper and LC filter, as inductor's average voltage in steady state is equal to zero, having charge time (t_{ON}) for given input voltage and discharging time (t_{OFF}) for an output voltage, boost circuit equation are calculated by,

$$V_{IN} \times t_{ON} = V_L \times t_{OFF} \quad (3.7)$$

and

$$V_{OUT} = V_{IN} + V_L \quad (3.8)$$

This gives relationship between output voltage and input voltage as

$$V_{OUT} = V_{IN} \times (1 + t_{ON}/t_{OFF}) \quad (3.9)$$

Where duty cycle (D) = $t_{ON}/(t_{ON} + t_{OFF})$ (3.10)

Then for the boost circuit equation can be further simplifies as:

$$V_{OUT} = V_{IN}/(1-D) \quad (3.11)$$

3.4.1 DESIGN OF CAPACITOR

Theoretically capacitor value is kept large to make output voltage constant. Practically ripple is calculated using voltage-current relation to design capacitance value.

$$\text{The change in capacitor charge is given by } |\Delta Q| = \frac{V_0}{R} (DT) = CV_0 \quad (3.12)$$

$$\text{Where ripple voltage is } \frac{\Delta V_0}{V_0} = \frac{D}{RCf} \quad (3.13)$$

$$\text{Capacitance with ripple voltage is } C = \frac{D}{R(\Delta V_0/V_0)f} \quad (3.14)$$

Critical capacitance is given where capacitor voltage waveform is just continuous by

$$C_c = \frac{D}{2Rf} \quad (3.15)$$

3.4.2 DESIGN OF INDUCTOR

$$\text{Average inductor current is } I_L = \frac{Vs}{R(1-D)^2} \quad (3.16)$$

$$\text{Inductance in terms of } \Delta i_L, \text{ i.e } L = \frac{VsDT}{\Delta i_L} = \frac{VsD}{\Delta i_L f} \quad (3.17)$$

Critical Inductance is given where the inductor current waveform is just continuous by

$$L_c = \frac{RD(1-D)2}{2f} \quad (3.18)$$

3.5 BUCK CONVERTER

A buck converter is a step-down DC-to-DC voltage converter, it consists of two power semiconductor (diode and transistor) switches and inductor and capacitor in series parallel combination.

$$\text{Output voltage of buck circuit is given by: } V_{\text{OUT}} = V_{\text{IN}} \times D \quad (3.19)$$

3.5.1 DESIGN OF INDUCTOR

$$\text{Average inductor current } I_L = \frac{V_0}{R} \quad (3.20)$$

$$\text{Inductor in terms of ripple current } \Delta i_L, \text{ is } L = \frac{V_0 (1-D)}{\Delta i_L f} \quad (3.21)$$

Critical Inductance is given where the inductor current waveform is just continuous by

$$L_c = \frac{R(1-D)}{2f} \quad (3.22)$$

3.5.2 DESIGN OF CAPACITOR

$$\text{The change in capacitor charge is } |\Delta Q| = \frac{T \Delta i_L}{8} \quad (3.23)$$

$$\text{Ripple voltage } \frac{\Delta V_0}{V_0} = \frac{1-D}{8LCf^2} \quad (3.24)$$

$$\text{Capacitance in terms of ripple voltage is } C = \frac{1-D}{8L(\Delta V_0/V_0)f^2} \quad (3.25)$$

Critical capacitance is gives where capacitor voltage waveform is just continuous by

$$C_c = \frac{1-D}{16Lf^2} \quad (3.26)$$

3.6 DC-DC CONVERTER FOR LDV

Design of two quadrant converter (full bridge) for (LDV), with an effective power of 3.3 kW, shown below in Fig 3.6.1. This converts DC source power bidirectionally as designed and controlled for lower voltage levels.

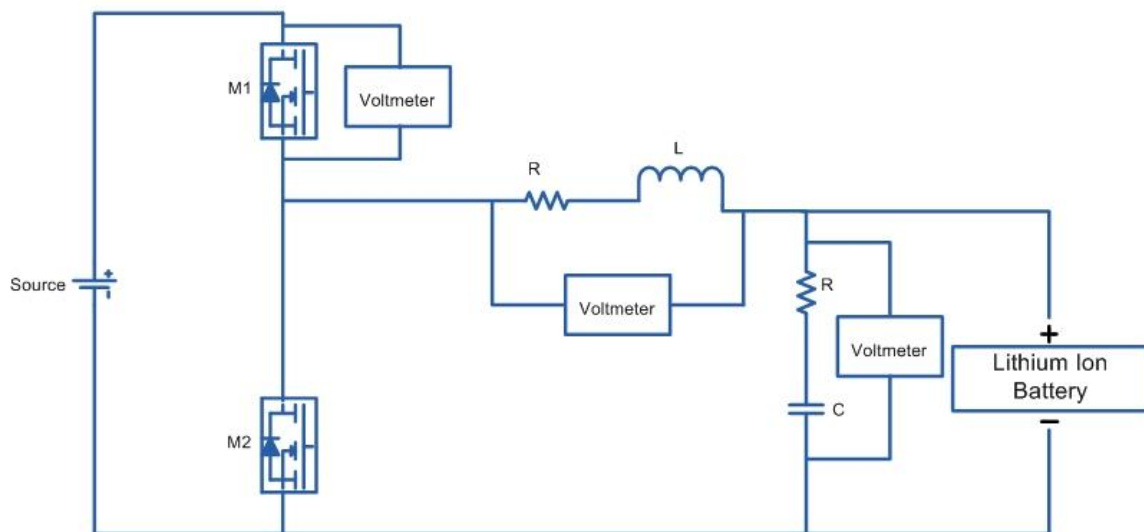


Figure 3.6.1: Two- quad (full bridge) converter for (LDV)

Here a power transfer takes place between two DC sources using type-C chopper controlled by switches i.e mosfet (M1, M2). This DC to DC converter system is designed for LDVs, which in turn set up a platform to cater and support auxiliary load, majorly DC load, for example this could be understood as supporting systems for instrument cluster and other entertainment devices empaneled in EVs or DC devices connected as per users requirement which may not be part of EVs.

3.6.1 MODELING PARAMETERS

Following table 3.6.1 represents the parameters used in modeling LDV DC/DC converter

Table 3.6.1: Modeling parameters for DC/DC converters

Circuit Element	Parameter	Values
Battery:	Nominal Voltage	24 V
	Rated Capacity	10 Ah
	Initial SOC	50%
	Battery response time	(1e-4) sec
Load (RL):	R	0.1 ohm
	L	1 mH
Load (RC):	R	0.1 m Ohm
	C	1 mF
DC source:	Voltage	48 V
Pulse generator:	Amplitude	1
	Period (sec)	(1e-4) sec
	Pulse Width	55
	Frequency	10 KHz
Charging Parameters Pulse Generator:	Amplitude	1
	Period	1*10^-4 sec
	Pulse Width	70
	SOC	50.24
	I _b	-86.88 amps
	V _b	30.62V
Discharging Parameters Pulse Generator:	Amplitude	1
	Period	1*10^-4 sec
	Pulse Width	40
	SOC	49.98
	I _b Current	9.157 amps
	V _b	25.34 V

3.6.2 DC-DC CONVERTER FOR LDV RESULTS

Result waveforms in figures 3.6.2a and 3.6.2b show battery parameters i.e SOC%, current and voltage for charging and discharging configuration of full bridge two quadrant converter for LDV respectively.

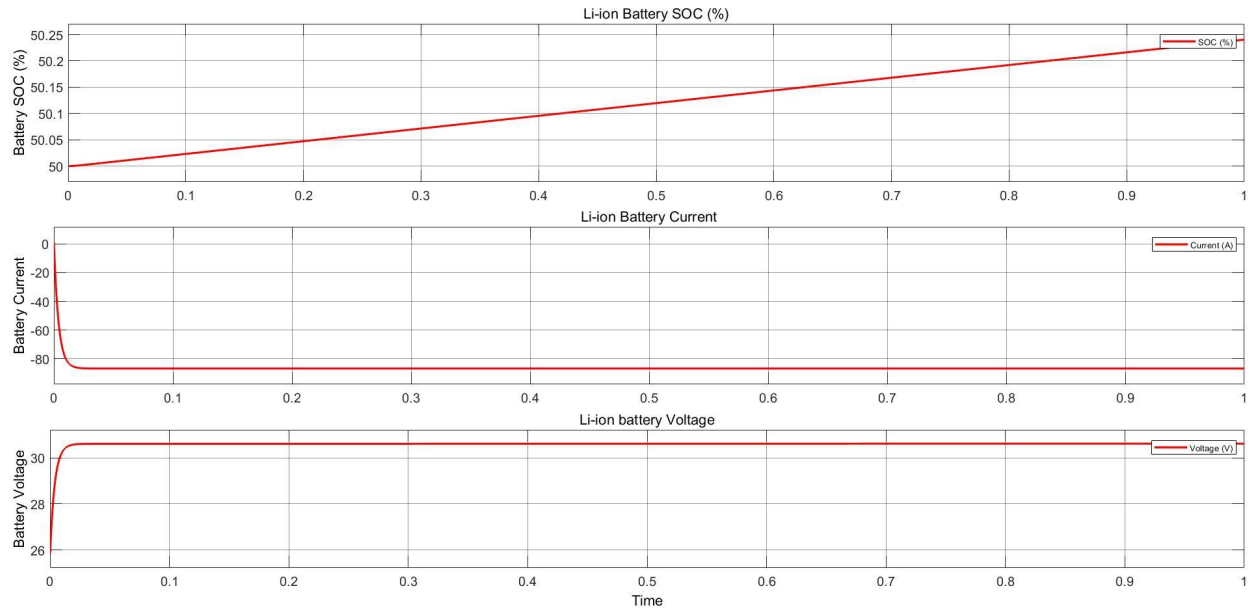


Figure 3.6.2a: Charging Output

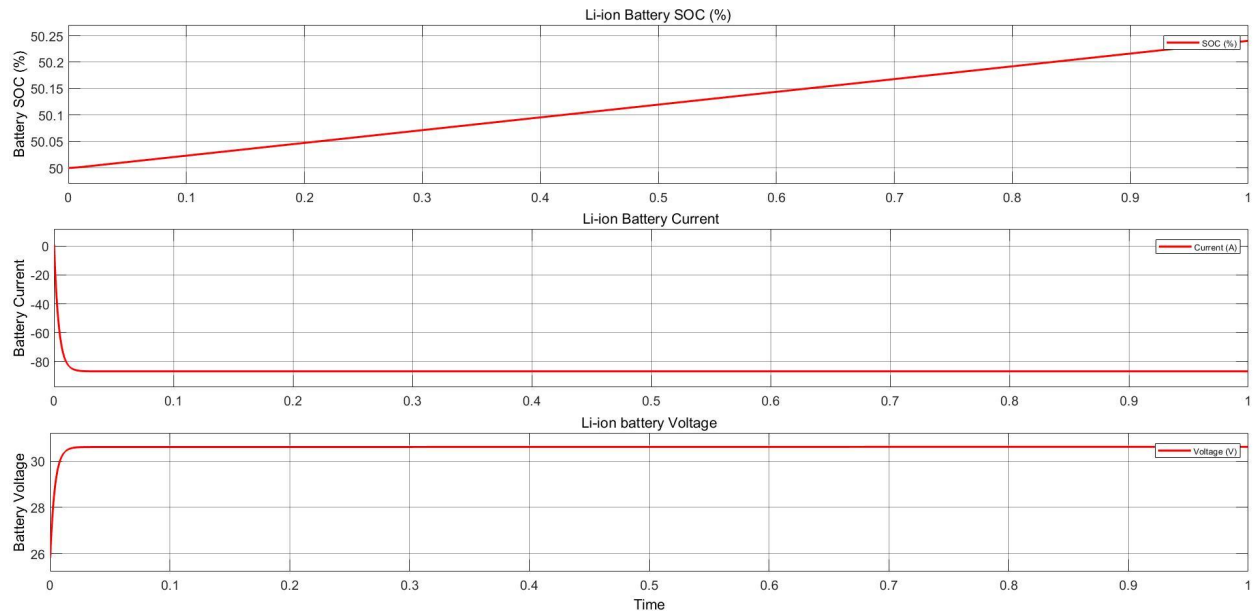


Figure 3.6.2b: Discharging Output

3.7 FULL BRIDGE TWO-QUADRANT CONVERTER FOR HDV

Design of full bridge two quadrant converter for Heavy-Duty Vehicles (HDV) in G2V topology, i.e 3 phase AC to DC coupled with DC link capacitor and DC/DC converter subsystem, which controlled using pulse generator to buck switch, this topology shown in Fig 3.7.1 have an effective power rating of 22 kW.

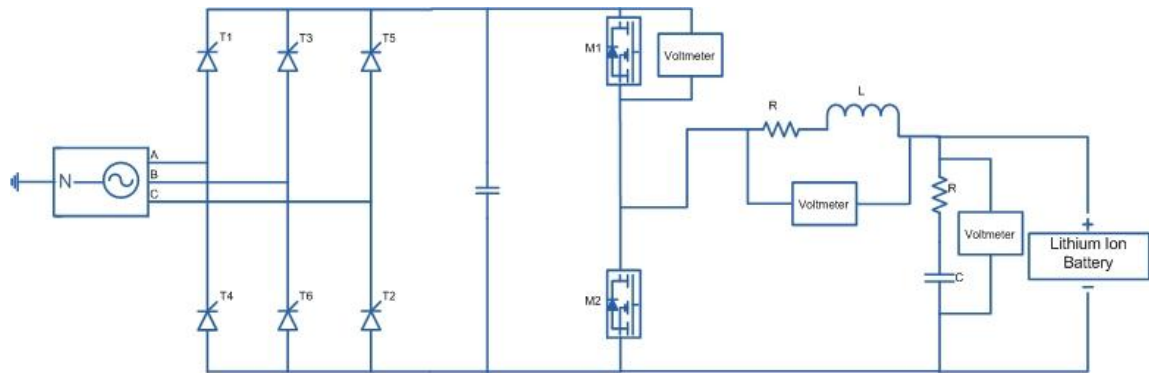


Figure 3.7.1: Circuit for full bridge two-Quadrant converter for Heavy-Duty Vehicles (HDV)

Here a net power transfer takes place between an AC grid and the battery (EV) via rectifier and type-C chopper. Switches at the rectifier side i.e thyristors are controlled to give a required voltage to the DC link bus so it can further be regulated via switches (M1, M2) to meet the battery conditions. This converter system is designed for heavy duty which forms the base for this project essentially supporting both the grid and battery (EV) connected.

3.7.1 MODELING PARAMETERS

Following table 3.7.1 represents the parameters used to simulate full bridge two-quad converter for HDV.

Table 3.7.1: Modeling parameters for two- quad HDV converter

Circuit Element	Parameter	Values
Battery:	Nominal Voltage	24 V
	Rated Capacity	10 Ah
	Initial SOC	50%
	Battery response time	(1e-4) sec
Load (RL):	Resistance (R)	0.1 ohm
	Inductance (L)	1 mH
Load (RC):	Resistance (R)	0.1 m Ohm
	Capacitance (C)	1 mF
3 Phase AC source:	Phase Voltage	230 Vrms
	Line Voltage	415 Vrms
	Frequency	50 Hz
Pulse generator (T1) :	Amplitude	1
	Period	0.02 sec
	Pulse Width	10
	Phase delay (sec)	(1.666e-3)+(5.388e-3)
Pulse generator (M1):	Amplitude	1
	Period	1e-4
	Pulse Width	70
	Phase delay	0
Current and Voltage ripple	ΔV_{max}	2%
	ΔI_{max}	10%

3.7.2 FULL BRIDGE TWO-QUAD CONVERTER FOR HDV RESULTS

Waveform in Fig 3.7.2 shows battery parameters i.e SOC%, current and voltage for charging configuration of full bridge two quadrant converter for Heavy-Duty Vehicles (HDV) in G2V topology.

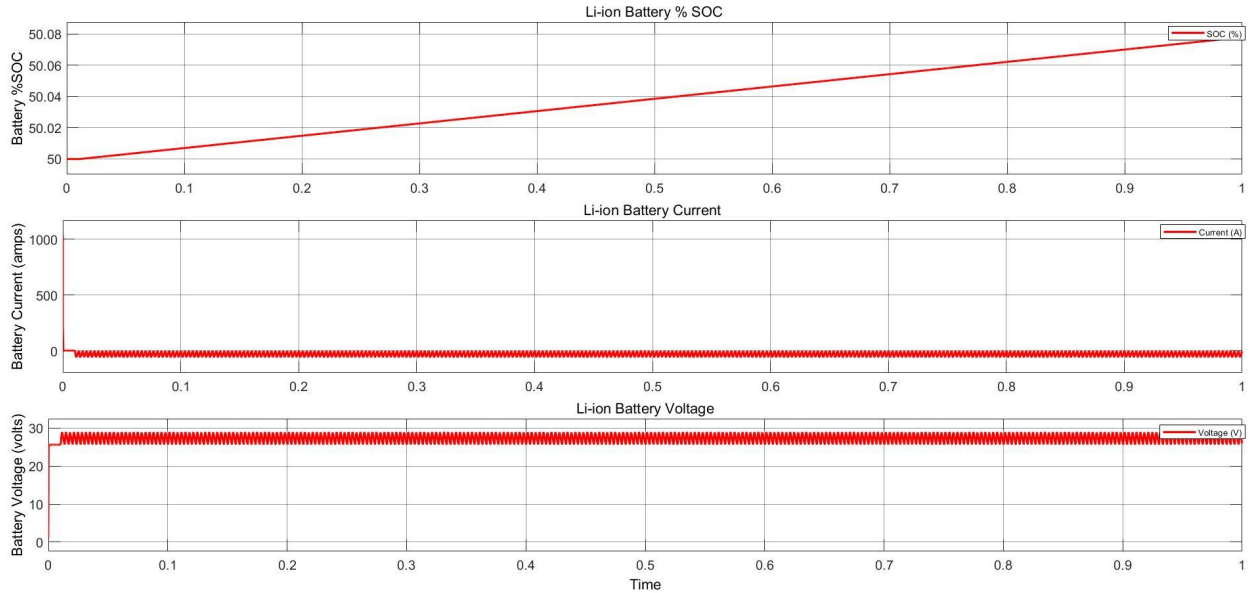


Figure 3.7.2: Charging Output

3.8 IMPLEMENTING REVERSE CHARGING

Design of full bridge two-quadrant converter for implementing Reverse charging that is in V2G topology, i.e DC to 3 phase AC, implementation shown in Fig 3.8.1. It has been designed both with balanced resistive load and with a grid LCL filter.

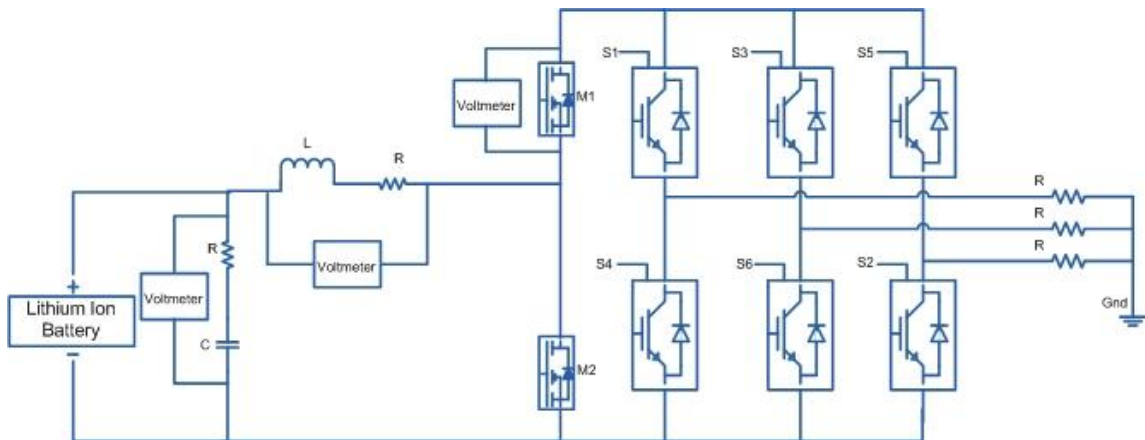


Figure 3.8.1: Implementation of V2G

3.8.1 MODELING PARAMETERS

Following table 3.8.1 represents the parameters used implementing reverse charging

Table 3.8.1: Modeling parameters for reverse charging

Circuit Element	Parameter	Values
Battery:	Nominal Voltage	24 V
	Rated Capacity	10 Ah
	Initial SOC	50%
	Battery response time	(1e-4) sec
Load (RL):	Resistance (R)	0.1 ohm
	Inductance (L)	1 mH
Load (RC):	Resistance (R)	0.1 m Ohm
	Capacitance (C)	1 mF
3 Phase AC source:	Phase Voltage	230 Vrms
	Line Voltage	415 Vrms
	Frequency	50 Hz
Pulse generator (T₁) :	Amplitude	1
	Period	0.02 sec
	Pulse Width	10
	Phase delay	(1.666e-3)+(5.388e-3)
Pulse generator (M₁):	Amplitude	1
	Period	1e-4
	Pulse Width	70
	Phase delay	0
Current and Voltage ripple	ΔVmax	2%
	ΔI _{max}	10%
Grid Filter	LCL filter	5mH, 30uF, 5mH

3.8.2 IMPLEMENTING REVERSE CHARGING RESULTS

Result waveform in Fig 3.8.2a shows battery parameters i.e SOC%, current and voltage for V2G topology (discharging configuration) of full bridge two-quadrant converter for implementing Reverse charging.

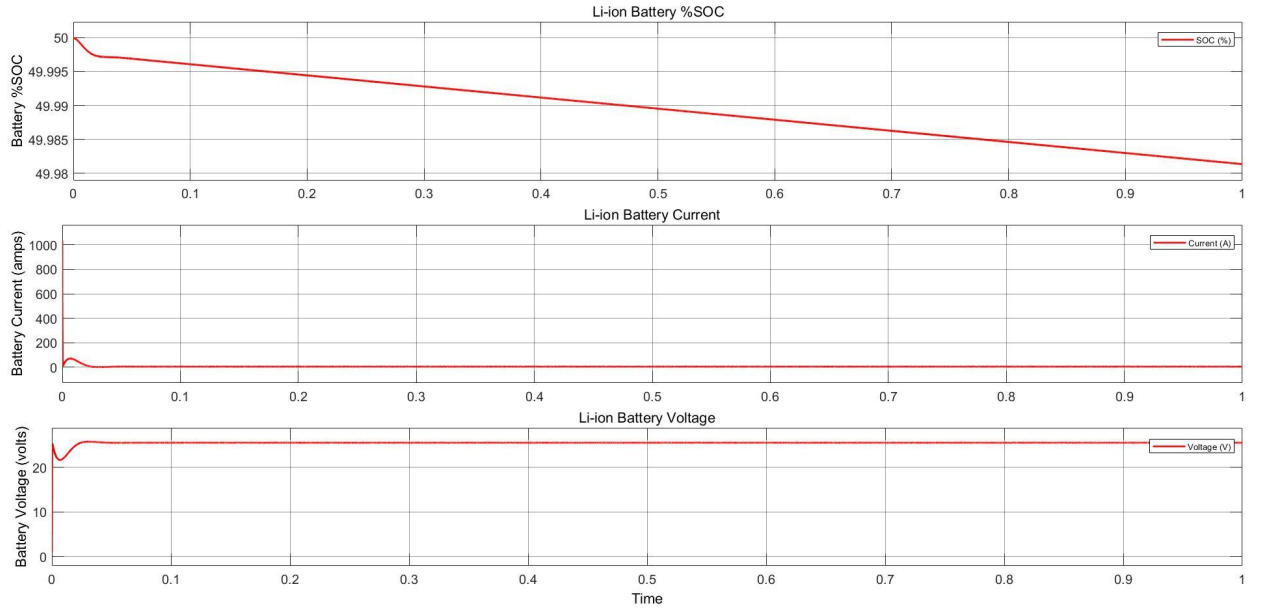


Figure 3.8.2a: Battery status after implementing V2G

Result waveforms respectively in figures 3.8.2b and 3.8.2c show output phase voltage (V_a , V_b & V_c) with and without LCL grid filter in V2G topology configuration.

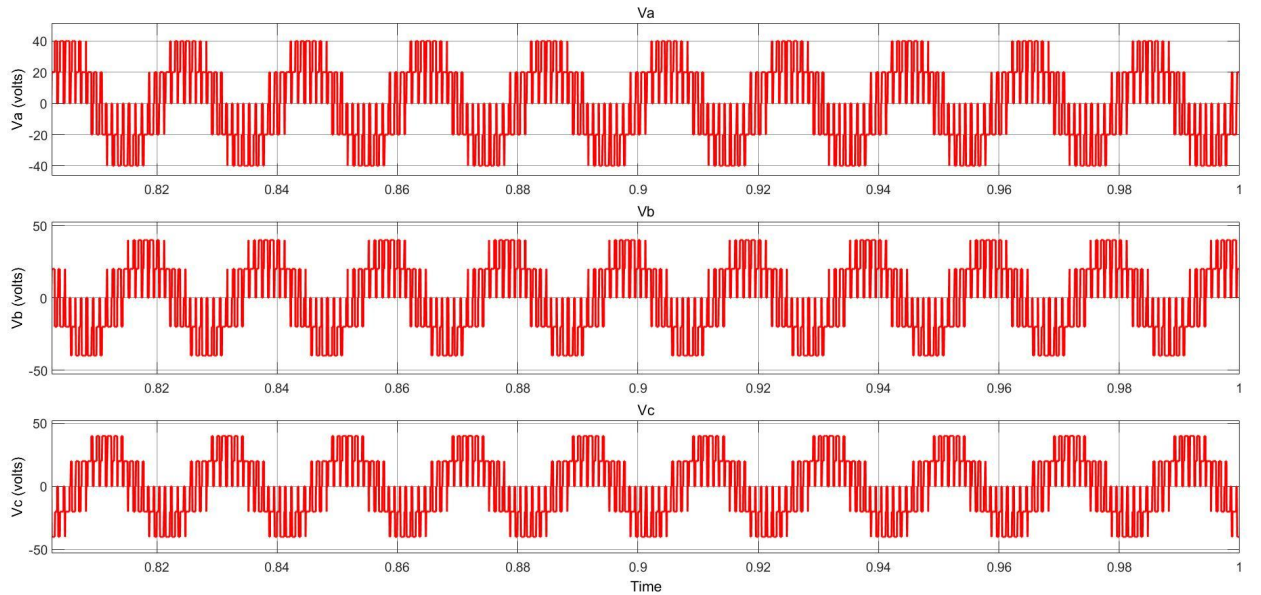


Figure 3.8.2b: Output phase with Resistive load without Filter voltage of V2G

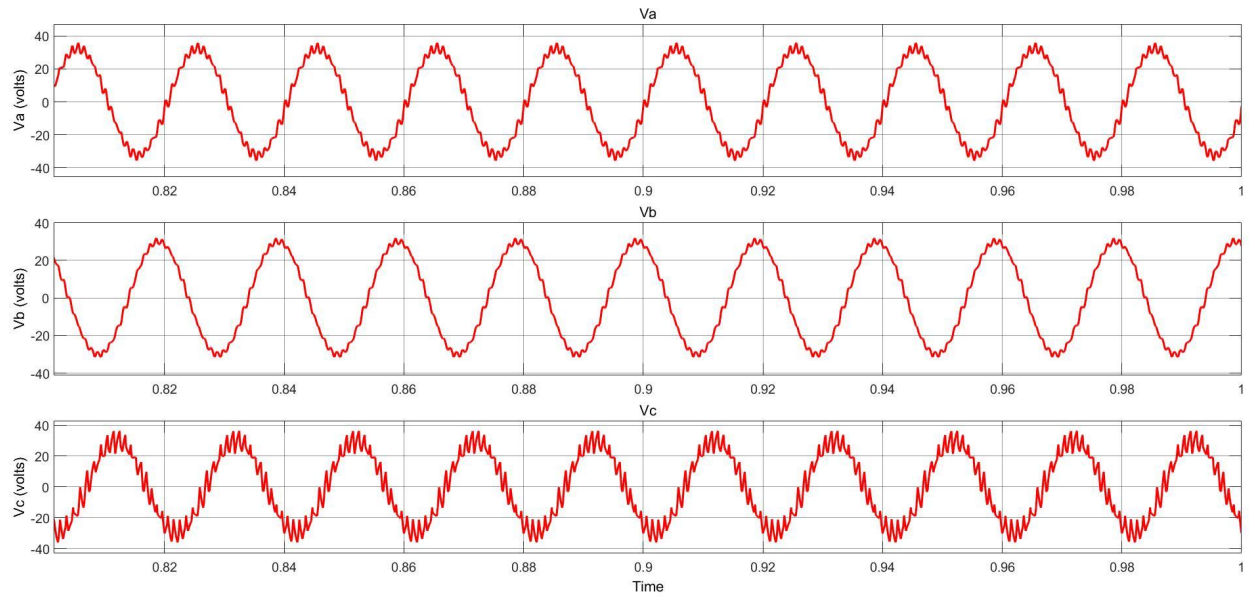


Figure 3.8.2c: Output phase voltage with LCL filter of V2G

4. DESIGN OF SUBSYSTEMS AND CONTROLLER

This chapter is focused on designing various subsystems and Phase-locked loop (PLL)-controllers for easy implementation of V2G-G2V technology without any manual intervention.

4.1 ON-BOARD / OFF-BOARD SUBSYSTEMS

On-board or Off-board subsystems are designed as per the requirement and availability of infrastructure as discussed earlier in section 1.3.1 which is On-Board vs. Off-Board Chargers. Here the aim is to create two subsystems, that is a three-phase bidirectional AC/DC rectifier and DC/DC regulator switches.

4.1.1 THREE PHASE BIDIRECTIONAL AC/DC CONVERTER SUBSYSTEM

A bidirectional AC/DC rectifier subsystem is basically a three phase bridge converter which makes the simulation simpler with added in-port pin and DC-link connection for PWM signal connection and grid connection which is shown in below Fig 4.1.1.

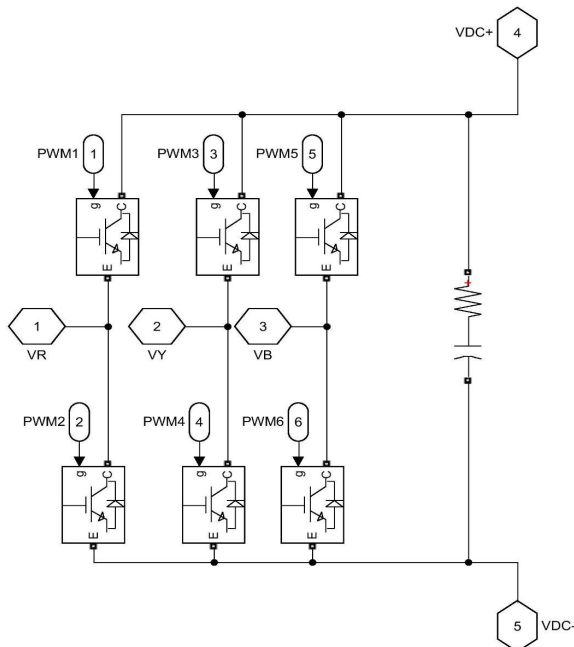


Figure 4.1.1: AC/DC Converter Subsystem

4.1.2 DC/DC CONVERTER SWITCHES SUBSYSTEM

A DC/DC regulator/converter subsystem works both as buck converter and boost converted essentially as a Type-C chopper which works in 1st and 2nd quadrant. This subsystem has input DC link connection with output EV integration connections as shown in Fig 4.1.2.

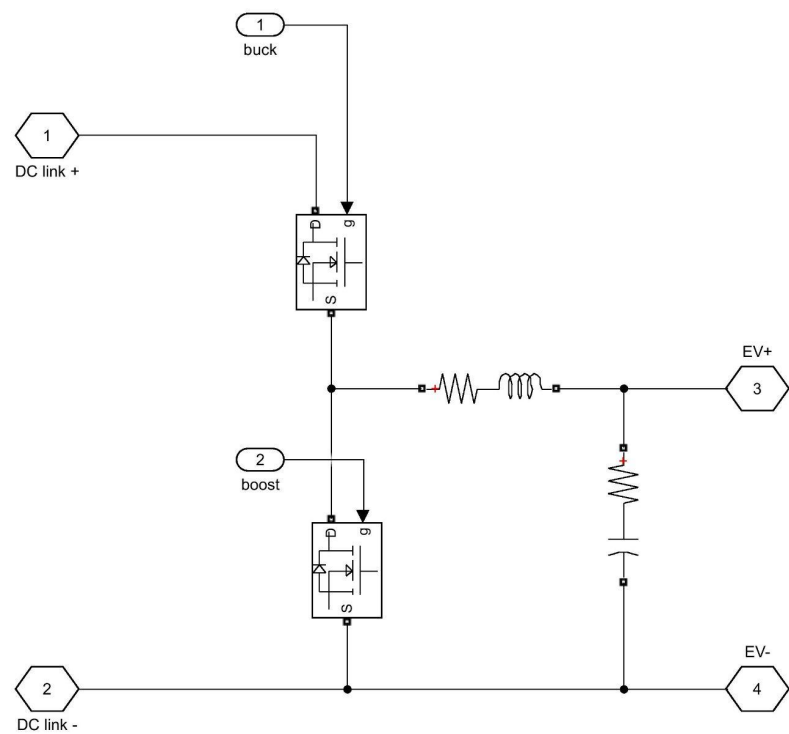


Figure 4.1.2: DC/DC converter subsystem

4.2 PHASE-LOCKED-LOOP (PLL) CONTROLLER

The PLL voltage and current controller is the main controlling mechanism installed in the project to control the flow of power from the grid to EVs and vice-versa. This mechanism creates the grid current reference for an internal closed-control loop to produce a switching pattern for the regulator/converter. PLL is used to synchronize the reference current to the grid voltage.

4.2.1 PLL - VOLTAGE CONTROLLER

The PLL voltage controller is designed initially with the grid measure values:

$$V_a = V_{\text{grid}} \sin(\omega t) \quad (4.1)$$

$$V_b = V_{\text{grid}} \sin(\omega t - 2\pi/3) \quad (4.2)$$

$$V_c = V_{\text{grid}} \sin(\omega t - 4\pi/3) \quad (4.3)$$

Then by using Clakes transform, phase voltages V_{abc} are transformed into $V_{\alpha\beta 0}$ and further by Park transform $V_{\alpha\beta 0}$ is converted into V_{dq0} frame as shown in below controlling block Fig 4.2.1a.

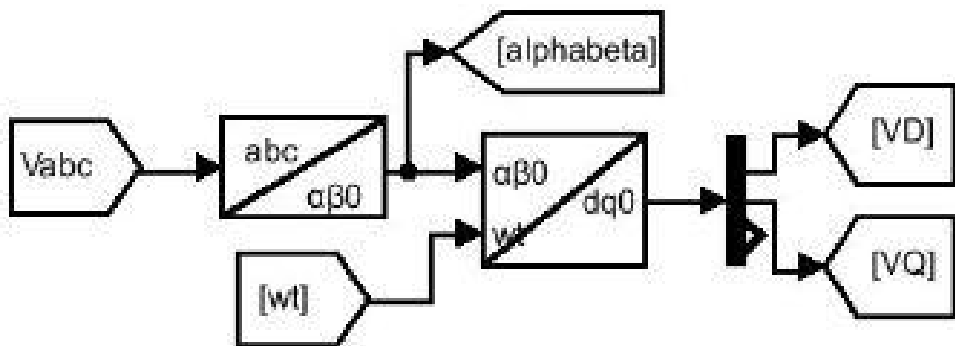


Figure 4.2.1a: V_{abc} converting into V_{dq0} frame

The values of V_d and V_q could be found using matrix multiplication shown in eq 4.4.

$$\begin{bmatrix} V_d \\ V_q \end{bmatrix} = \frac{2}{3} \begin{bmatrix} \cos(\theta) & \cos(\theta - 2\pi/3) & \cos(\theta + 2\pi/3) \\ -\sin(\theta) & -\sin(\theta - 2\pi/3) & -\sin(\theta + 2\pi/3) \end{bmatrix} \begin{bmatrix} V_a \\ V_b \\ V_c \end{bmatrix} \quad (4.4)$$

Then a closed loop is formed using “Vabc” as in input and converting it into dq0 frame and further wt as output and feedback to make reference Vq=0 (required condition to be achieved for phase lock), here PI controller is taken to be (10,50000), as shown in below block diagram Fig 4.2.1b.

This helps in generating current reference signal with help of output wt which are,

$\sin(wt)$ = Active component reference

$\cos(wt)$ = Reactive component reference

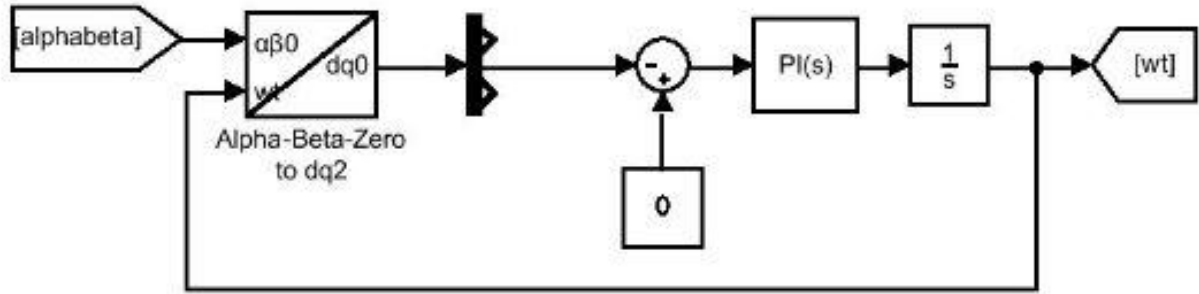


Figure 4.2.1b: PLL closed loop

For Active power injection the current should be in phase with reference voltage and for reactive power injection the current should be 90° out of phase with reference current

4.2.2 PLL - CURRENT CONTROLLER

The grid current I_a , I_b and I_c , are converted to dq0 frame as depicted in the below Fig 4.2.2a.

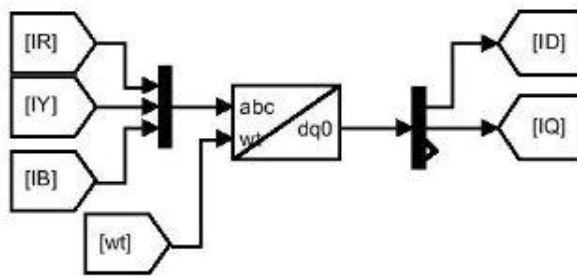


Figure 4.2.2a: I_{RYB} converted to I_{dq0}

Then two control blocks, one with active current (I_d) reference and other one with reactive current (I_q) references are created.

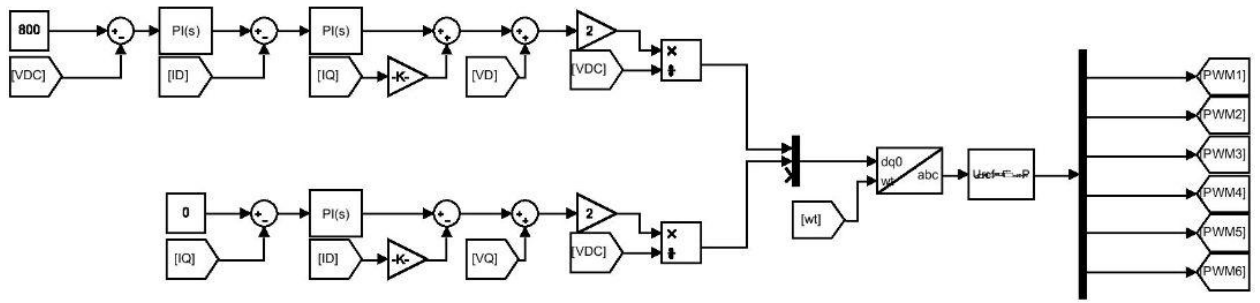


Figure 4.2.2b: PLL current controller

Here the active current controller DC-link voltage (VDC) is compared with VDC_{ref} which is set at 800 volts. It generates I_d_{ref} through PI (0.5,5) controller, further it is compared with actual I_d (from abc to dq0 transform). This is used to generated U_d through PI (25,500) controller which is added with $(V_d + L\omega I_q)$ and multiplied by $(2/VDC)$ to give modulation index m_d as $(V_d = m_d * VDC/2)$.

Again for the reactive current controller I_q (from abc to dq0 transform) is compare with $I_{q_{ref}} = 0$, the error then though PI (25,500) is U_q is added $(V_d - L\omega I_d)$ and multiplied by $2/VDC$ to give modulation index m_q as $(V_q = m_q * VDC/2)$.

Then m_d and m_q are converted back to abc frame to generate PWM signal from 2-level PWM generator (10KHz) using Sine PWM switching with unipolar scheme for the three phase bidirectional AC/DC Converter Subsystem in-ports [S1, S2, S3, S4, S5, S6] as designed in above figure 4.2.2b.

4.2.3 POWER FLOW USING PLL CONTROLLER

Active current and reactive current transfer/injection is explained with the help of phasor sum of inverter, grid and inductor voltage drop, for V2G mode of operation inverter voltage is given by phasor sum as $\bar{V}_{INV} = \bar{V}_G + \bar{V}_L$. (4.5)

Here the grid is assumed to be inductive in nature.

case(i):

For active current transfer, grid current and grid voltage should be in phase, and inductor voltage leads the grid current by 90° as shown in phase diagram 4.2.3a

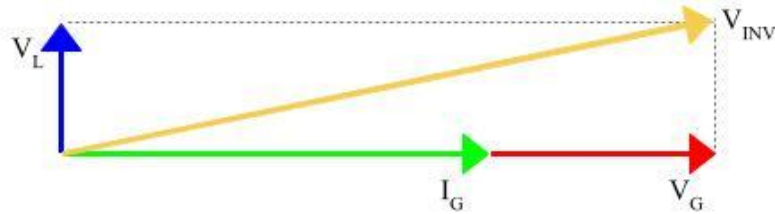


Figure 4.2.3a: Active current flow phasor diagram

This phasor implies that \bar{V}_{INV} (Inverter voltage) leads \bar{V}_G (Grid voltage) by some angle and has similar magnitude, i.e $|\bar{V}_G| \approx |\bar{V}_{INV}|$ and $\angle \bar{V}_{INV} - \angle \bar{V}_G = \delta$ (small value). Here δ defines the direction of flow of current. In this case Active power is given by $P = \frac{V_{inv} * V_g}{\omega L} \sin(\delta)$. (4.6)

case(ii):

For lagging reactive current transfer/injection, grid current lags grid voltage by 90° , resulting the inductor voltage to be in phase with grid voltage whose sum gives inverter voltage.

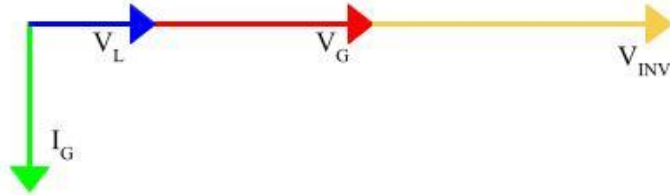


Figure 4.2.3b: Phasor diagram for lagging reactive current transfer

Above phasor diagram shows that \bar{V}_{INV} (Inverter voltage) is greater than \bar{V}_G (Grid voltage) with zero phase difference, i.e $|\bar{V}_{INV}| > |\bar{V}_G|$ and $\angle \bar{V}_{INV} = \angle \bar{V}_G$. In this case Reactive power is given by $Q = \frac{(V_{inv} - V_g) * V_g}{\omega L}$. (4.7)

case(iii):

For leading reactive current transfer/injection, grid current leads grid voltage by 90° , resulting the inductor voltage to be out of phase with grid voltage by 180° whose vector/phasor sum gives inverter voltage.

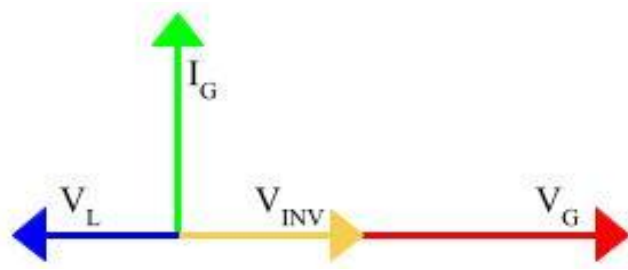


Figure 4.2.3c: Phasor diagram for leading reactive current transfer

Resulting phasor diagram shows that \bar{V}_{INV} (Inverter voltage) is less than \bar{V}_G (Grid voltage) with zero phase difference, i.e $|\bar{V}_{INV}| < |\bar{V}_G|$ and $\angle \bar{V}_{INV} = \angle \bar{V}_G$.

Different magnitude and angle conditions of current flow in the grid is present in the form of table 4.2.3 below.

Table 4.2.3: Condition for flow of grid current

Current injection	Magnitude condition	Angle condition
Active current	$ \bar{V}_G \approx \bar{V}_{INV} $	$\angle \bar{V}_{INV} - \angle \bar{V}_G = \delta$
Reactive current [lagging]	$ \bar{V}_{INV} > \bar{V}_G $	$\angle \bar{V}_{INV} = \angle \bar{V}_G$
Reactive current [leading]	$ \bar{V}_{INV} < \bar{V}_G $	$\angle \bar{V}_{INV} = \angle \bar{V}_G$

4.2.4 BATTERY CHARGING AND DISCHARGING CONTROLLER

The battery controller depends on the reference current set at 30 Amps for charging and -30 Amps for discharging.

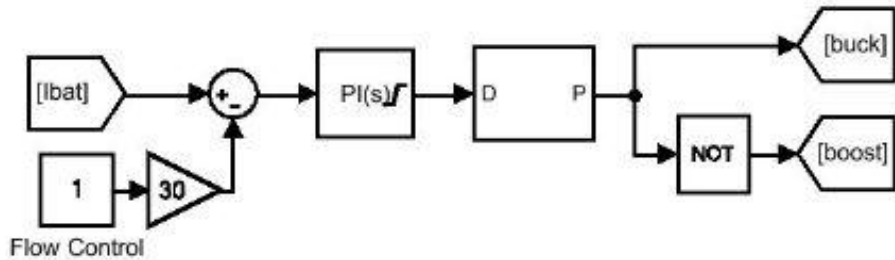


Figure 4.2.4a. Battery charging controller

The battery charging controller as shown in above figure 4.2.4a, take I_{bat} (actual battery current) then compare it with $I_{bat_{ref}}$ ($=30$ Amps for charging), Then through PI (0.005,10) controller with limiter (0,0.95) to DC-DC PWM generator (10KHz) generates signal which is fed to buck and boost mosfets of DC/DC converter switches subsystem.

Similarly, for battery discharging controller I_{bat} is compared with negative $I_{bat_{ref}}$ (i.e. $=-30$ Amps) apart from generating signals for DC/DC converter switches subsystems which is explained above.

The battery controller responses fed to PWM DC-DC converter are shown in figures 4.2.4a, 4.2.4b, and 4.2.4c, for V2G, G2V and abrupt change in operation respectively.

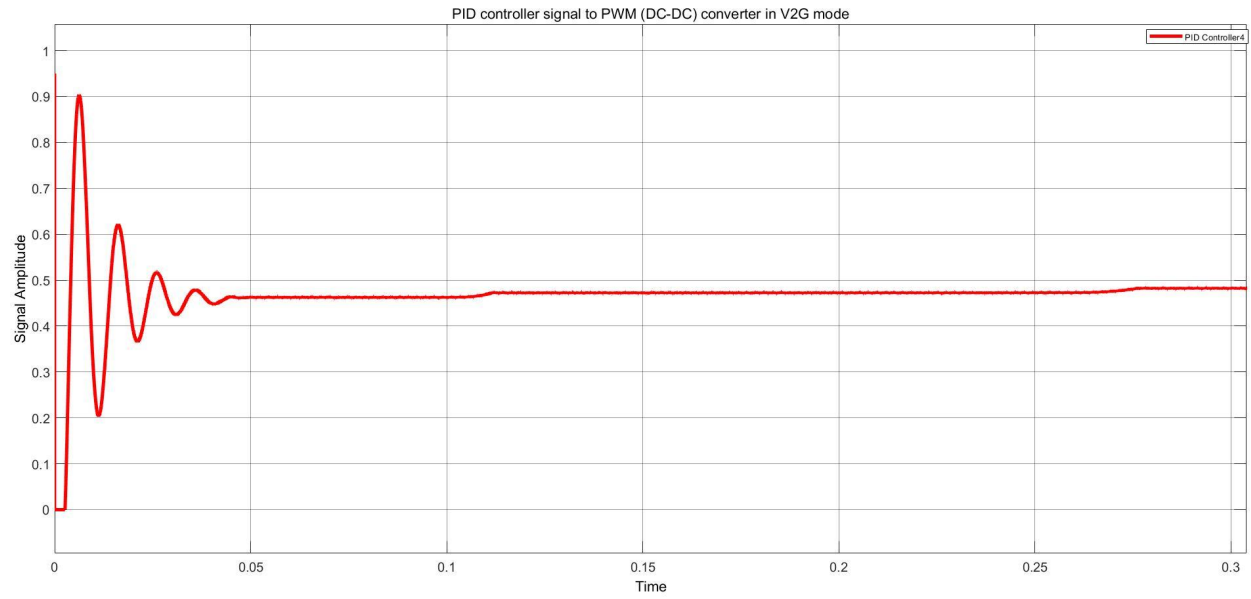


Figure 4.2.4b: Battery controller responses in V2G operation

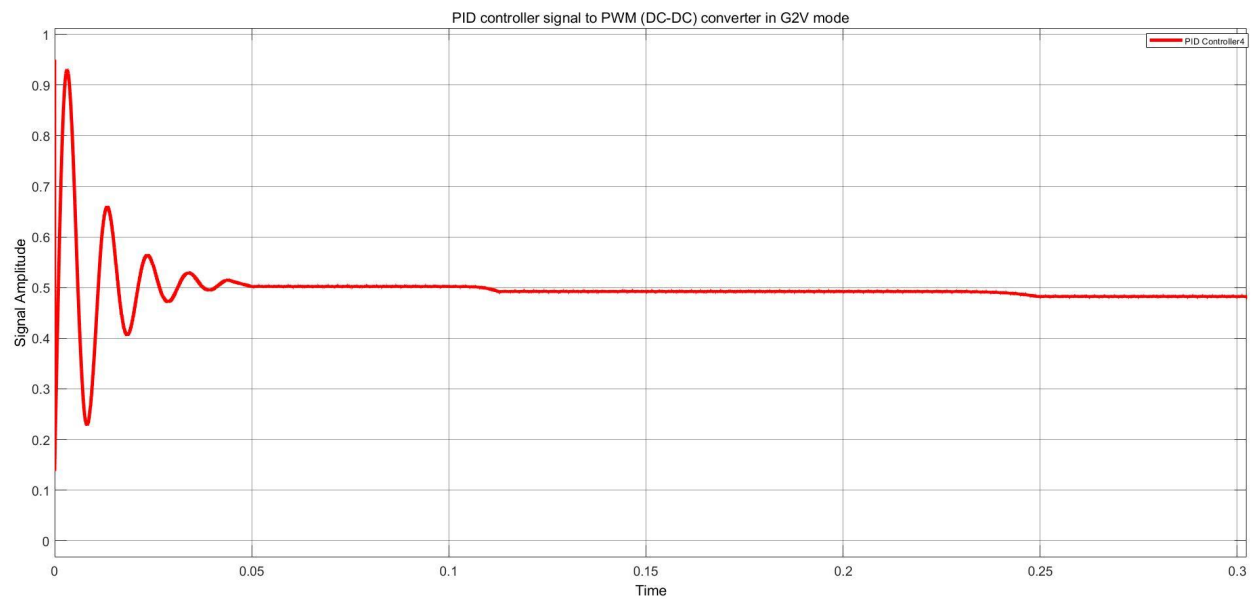


Figure 4.2.4c: Battery controller responses in G2V operation

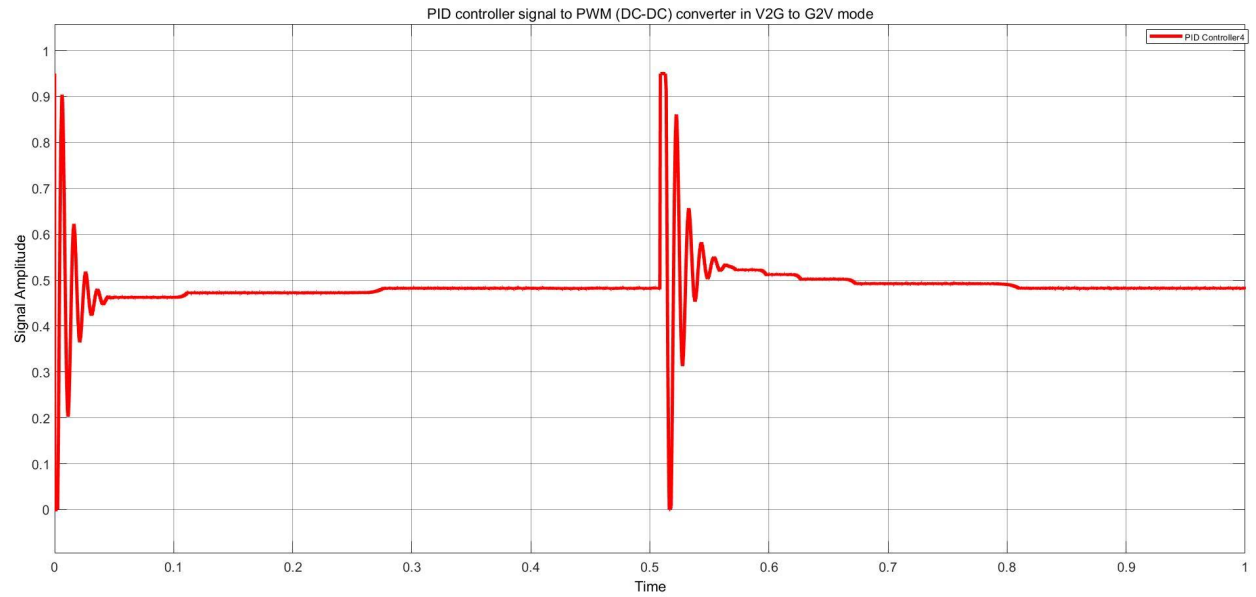


Figure 4.2.4d: Battery controller responses at abrupt change of operation from V2G to G2V

5. IMPLEMENTING AUTONOMOUS V2G-G2V CONTROLLED OPERATION

This chapter explains about the MATLAB/SIMULINK model designed for V2G-G2V operation with a toggle switch eliminating human or any manual intervention and with parallel operation of EVs (batteries). This section also deals with %THD performance of the system designed.

5.1 V2G-G2V OPERATION CONTROLLED WITH A TOGGLE SWITCH

Simulink model for V2G-G2V operation controlled via a toggle switch is shown below Fig 5.1.1, this model is integrated with both the subsystems explained in section 4.1. This model is controlled by a PLL-controller as discussed in section 4.2 with a toggle switch to switch between the operation of V2G to G2V or vice-versa.

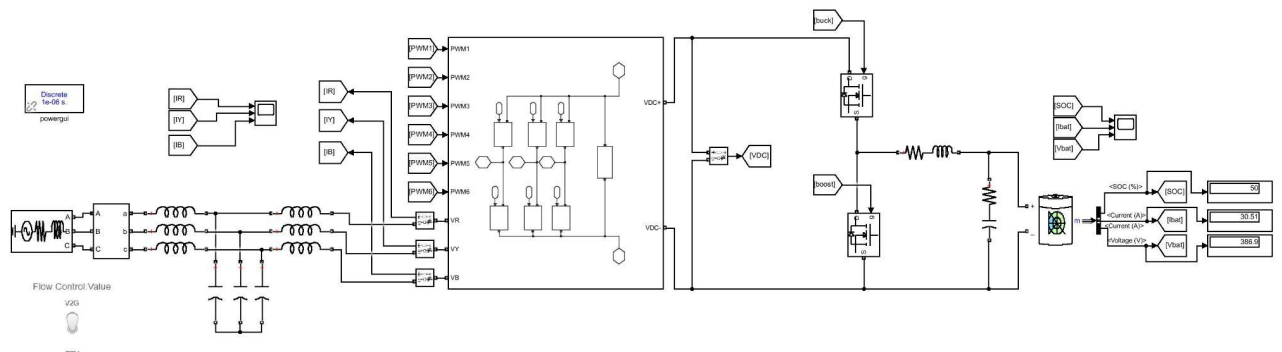


Figure 5.1.1: Simulink model for V2G-G2V operation controlled via a toggle switch

5.1.1 MODELING PARAMETERS

Following table 5.1.1 represents the parameters used in modeling of automated V2G-G2V operation.

Table 5.1.1: Modeling parameters for automated V2G-G2V topology.

Circuit Element	Parameter	Values
Battery:	Nominal Voltage	360 V
	Rated Capacity	300 Ah
	Initial SOC	50%
	Battery response time	1 sec
Load (RL):	Resistance (R)	0.1 m ohm
	Inductance (L)	20 mH
Load (RC):	Resistance (R)	0.1 m Ohm
	Capacitance (C)	0.625 mF
3 Phase AC source:	Phase Voltage	230 Vrms
	Line Voltage	415 Vrms
	Frequency	50 Hz
Grid Filter	LCL filter	5mH, 30uF, 5mH
DC link	Capacitor	5600 uF
	Resistor	1 m ohm
Switching Frequency	For IGBT	10 KHz

5.1.2 WORKING OPERATIONS

For V2G operation the current reference is +30 amps, this gives the positive active power which means that active power flow is out i.e from battery to grid, having both Voltage and Current are in phase. This lead to injection of the power to Grid and decrease in %SOC of the battery

On the contrary, for G2V operation the current reference is -30 amps, providing a negative active power implying active power flow is from grid to battery, having both voltage and current are out of phase by 180°. This leads to G2V operation, battery gets charged i.e %SOC increases.

5.1.3 V2G RESULTS

Figures 5.1.3a, 5.1.3b, and 5.1.3c, below shows battery performance, grid three phase current-voltage and DC-link voltage respectively in V2G operation.

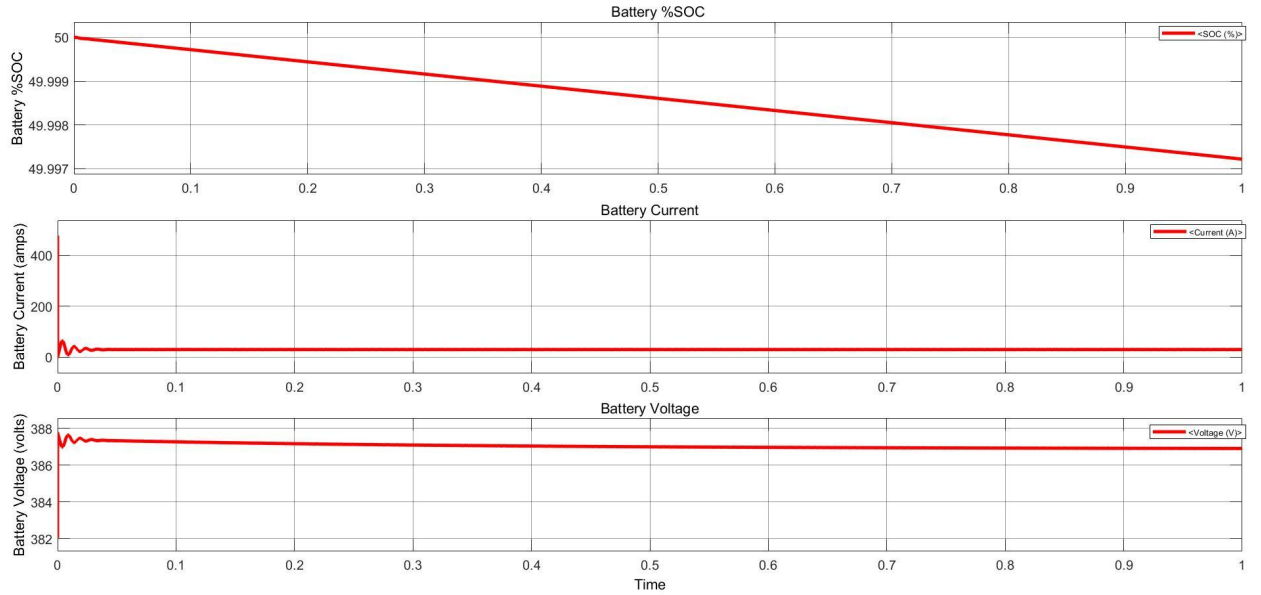


Figure 5.1.3a: Battery performance in V2G mode

Here, in Fig 5.1.3b, it is observed that the grid voltage and current waveforms are in phase with each other, which validates the V2G grid operation of the topology. This condition of zero phase difference implies that a proper phase-lock loop is controlled and synchronized.

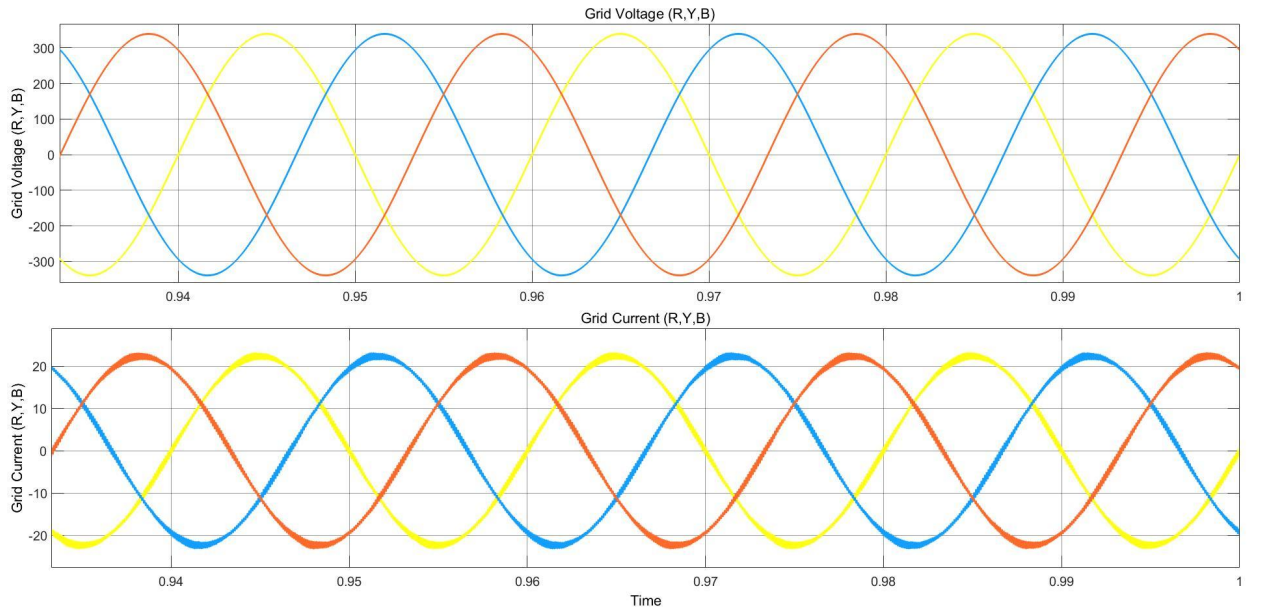


Figure 5.1.3b: Three phase grid voltages and current in V2G mode

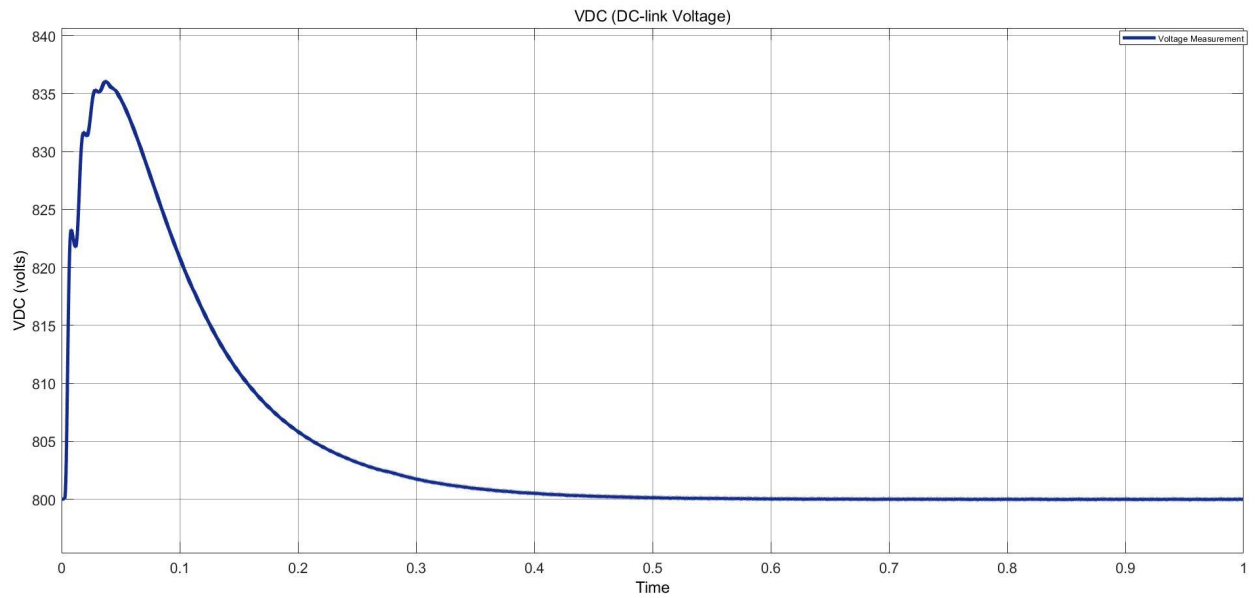


Figure 5.1.3c: DC link voltage in V2G mode

5.1.4 G2V RESULTS

Figures 5.1.4a, 5.1.4b, and 5.1.4c, below shows battery performance, grid three phase current-voltage and DC-link voltage respectively in G2V operation.

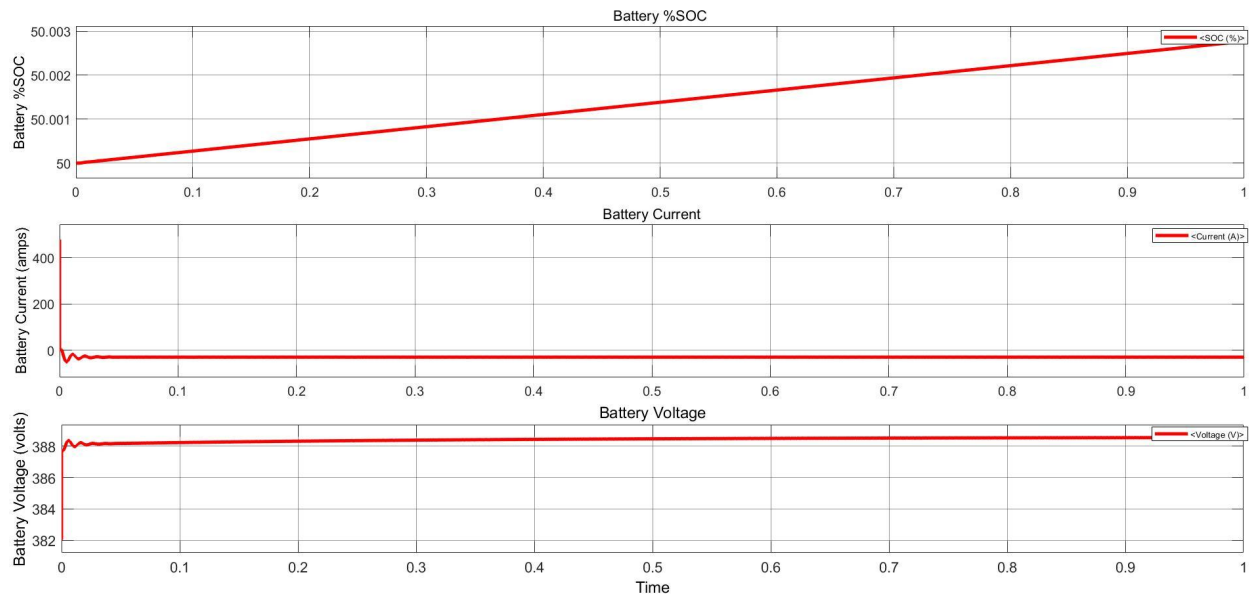


Figure 5.1.4a: Battery performance in G2V mode

Here, in Figure 5.1.4b, it is observed that the grid voltage and current waveforms are out of phase with each other by an angle of 180^0 , which validates the G2V grid operation of the topology.

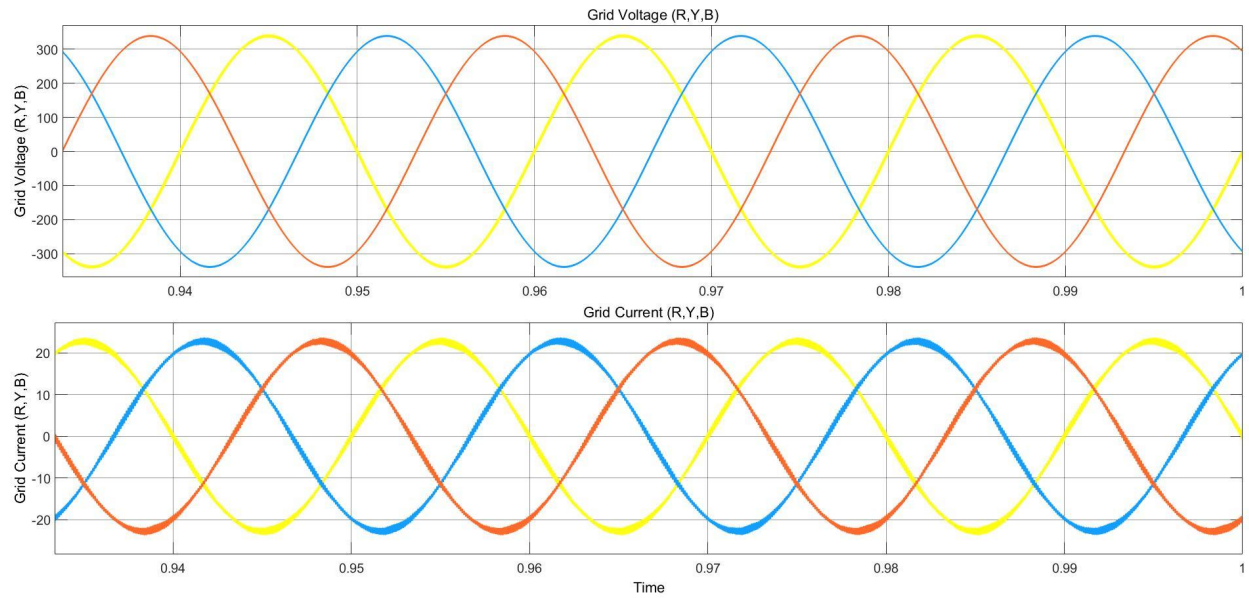


Figure 5.1.4b: Three phase grid voltages and current in G2V mode

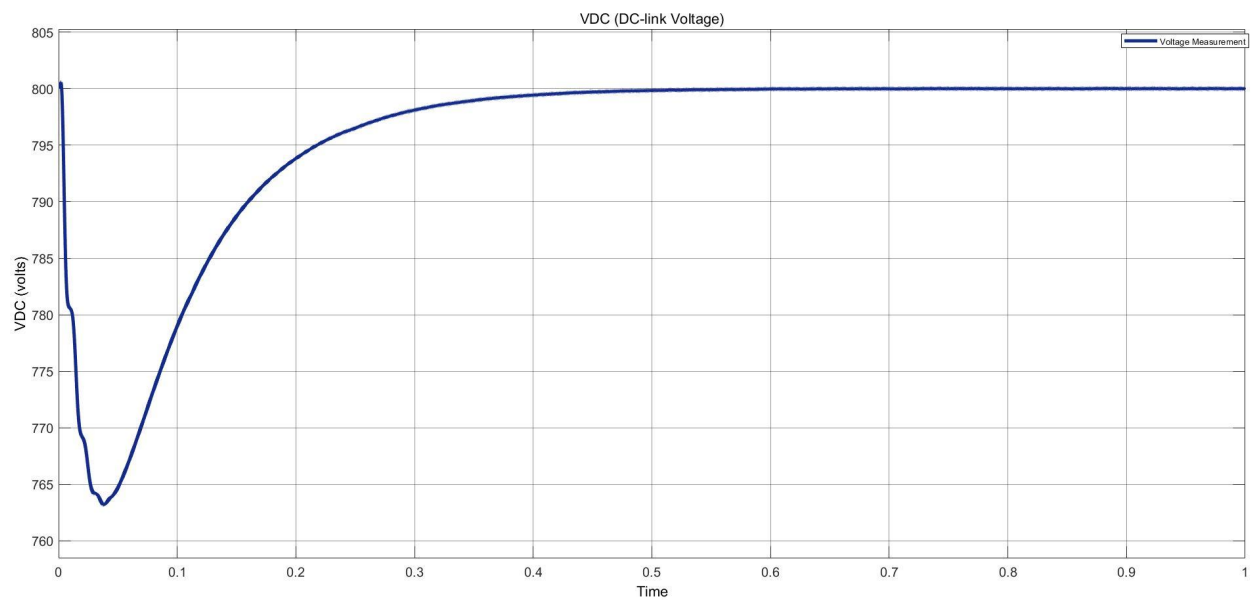


Figure 5.1.4c: DC link voltage in G2V mode

5.1.5 ABRUPT CHANGE IN OPERATIONS RESULTS

Figures 5.1.5a, 5.1.5b, and 5.1.5c, below shows battery performance, grid three phase current-voltage and DCLink voltage respectively when an abrupt change of operation occurs from V2G to G2V.

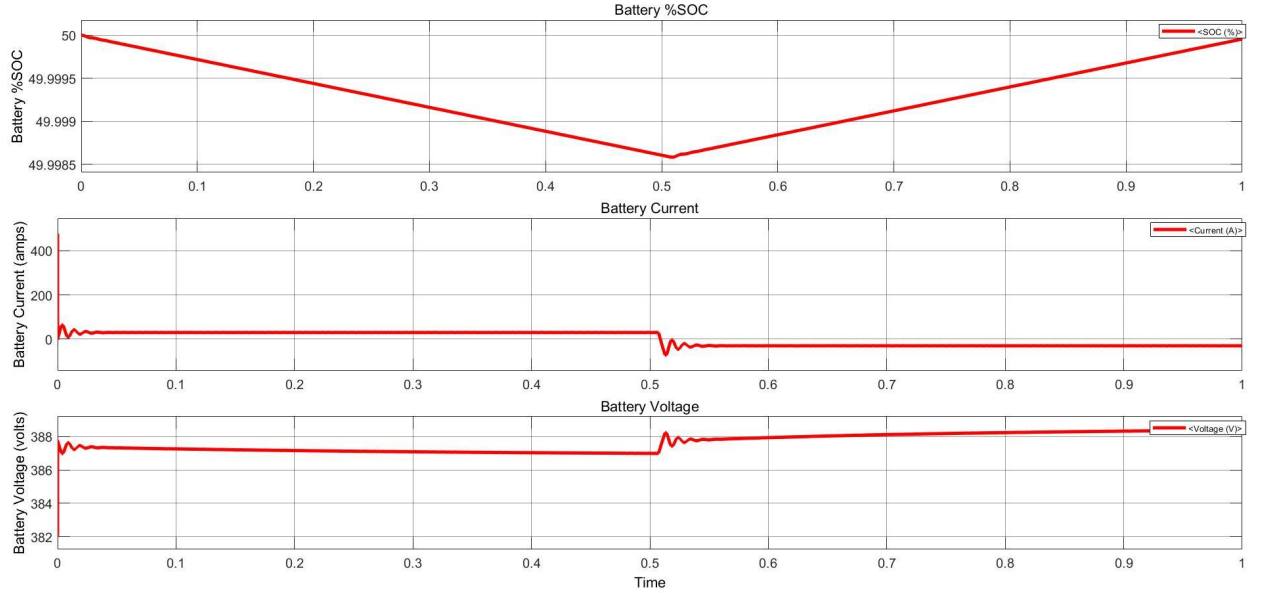


Figure 5.1.5a: Battery performance when V2G is changed to G2V mode

It is observed in Fig 5.1.5b, that when the operation from V2G is changed to G2V abruptly then the PLL-controls the process of synchronization very swiftly, which while maintaining phase lock of 0^0 in V2G is now maintaining a 180^0 phase-lock in G2V operation.

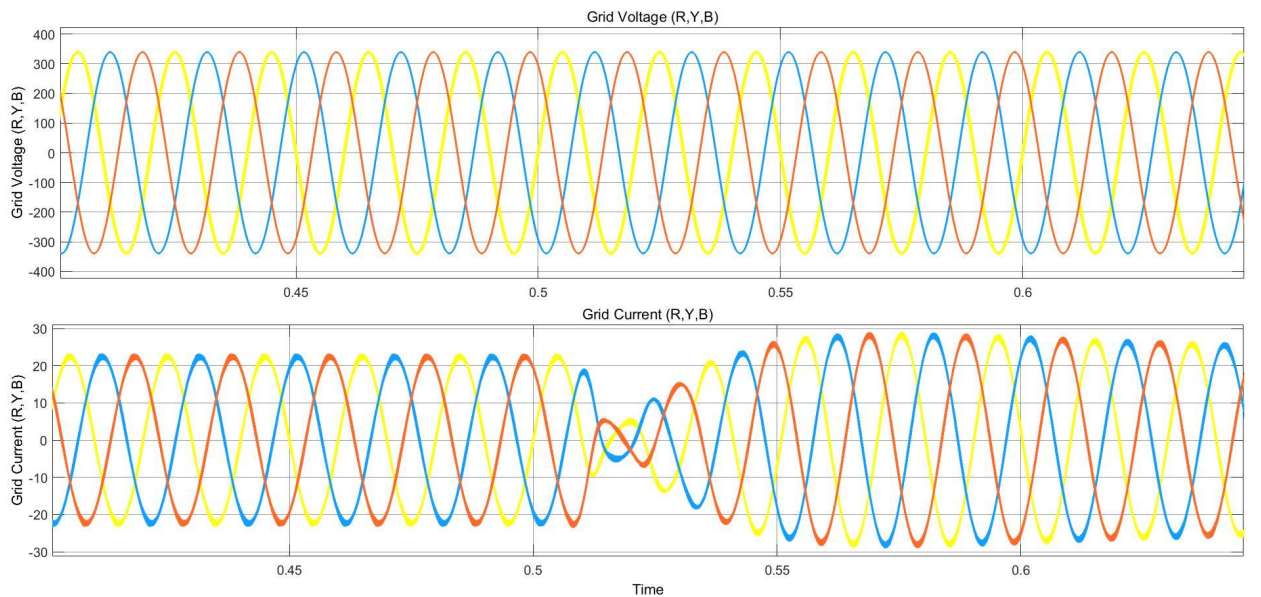


Figure 5.1.5b: Three phase grid voltages and current at change of operating mode

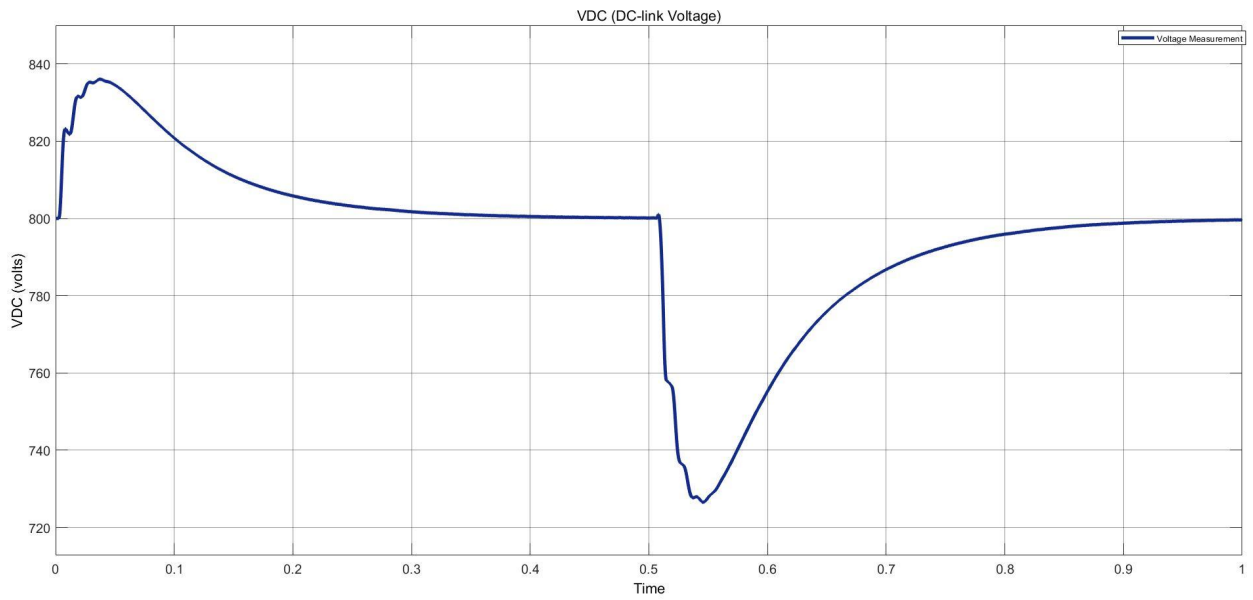


Figure 5.1.5c: DC link voltage at change of operating mode

5.2 V2G-G2V WITH PARALLEL OPERATION OF BATTERIES

The extended V2G-G2V simulink model with parallel operation of batteries (indeed EVs) operating mode controlled via a toggle switch is shown below Fig 5.2.1, this model is an extension of the model simulated in section 5.1.

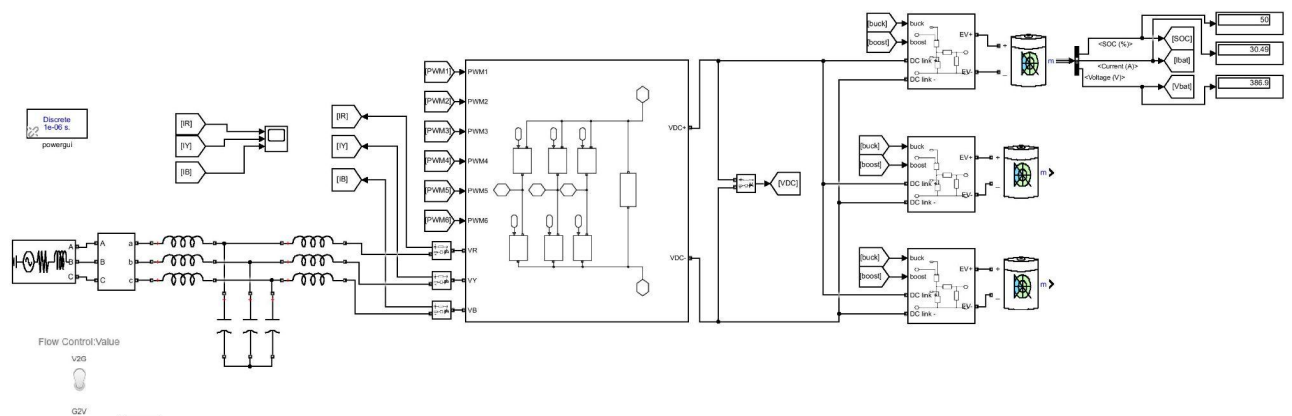


Figure 5.2.1: Simulink model for V2G-G2V topology with parallel operation of batteries

5.2.1 MODELING PARAMETERS

Following table 5.2.1 represents the parameters used in modeling of automated V2G-G2V topology with parallel operation of batteries .

Table 5.2.1: Modeling parameters for V2G-G2V with parallel operation of batteries

Circuit Element	Parameter	Values
Battery:	Nominal Voltage	360 V
	Rated Capacity	300 Ah
	Initial SOC	50%
	Battery response time	1 sec
Load (RL):	Resistance (R)	0.1 m ohm
	Inductance (L)	20 mH
Load (RC):	Resistance (R)	0.1 m Ohm
	Capacitance (C)	0.625 mF
3 Phase AC source:	Phase Voltage	230 Vrms
	Line Voltage	415 Vrms
	Frequency	50 Hz
Grid Filter	LCL filter	5mH, 30uF, 5mH
DC link	Capacitor	5600 uF
	Resistor	1 m ohm
Switching Frequency	For IGBT	10 KHz

5.2.2 V2G WITH PARALLEL OPERATION RESULTS

Figures 5.2.2a and 5.2.2b, below shows the grid three phase voltage-current and DC-link voltage respectively in V2G mode with parallel operation of batteries (EVs), the grid voltage and the current waveforms are in phase with each other validating the same operation.

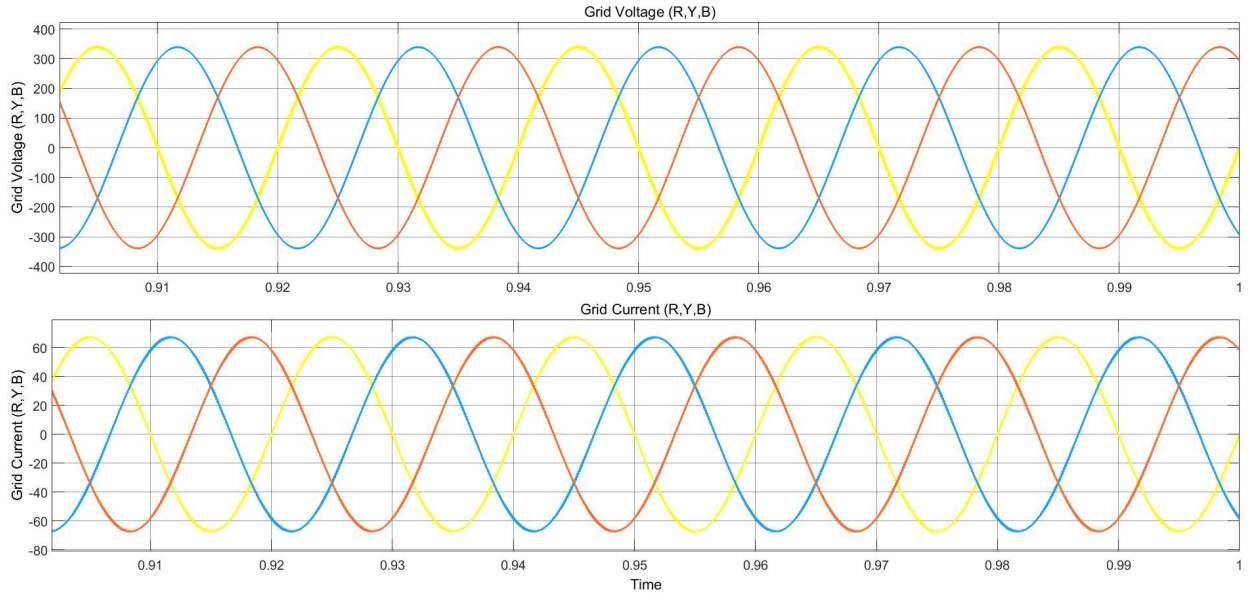


Figure 5.2.2a: Three phase grid voltages and current in V2G mode with parallel operation of batteries

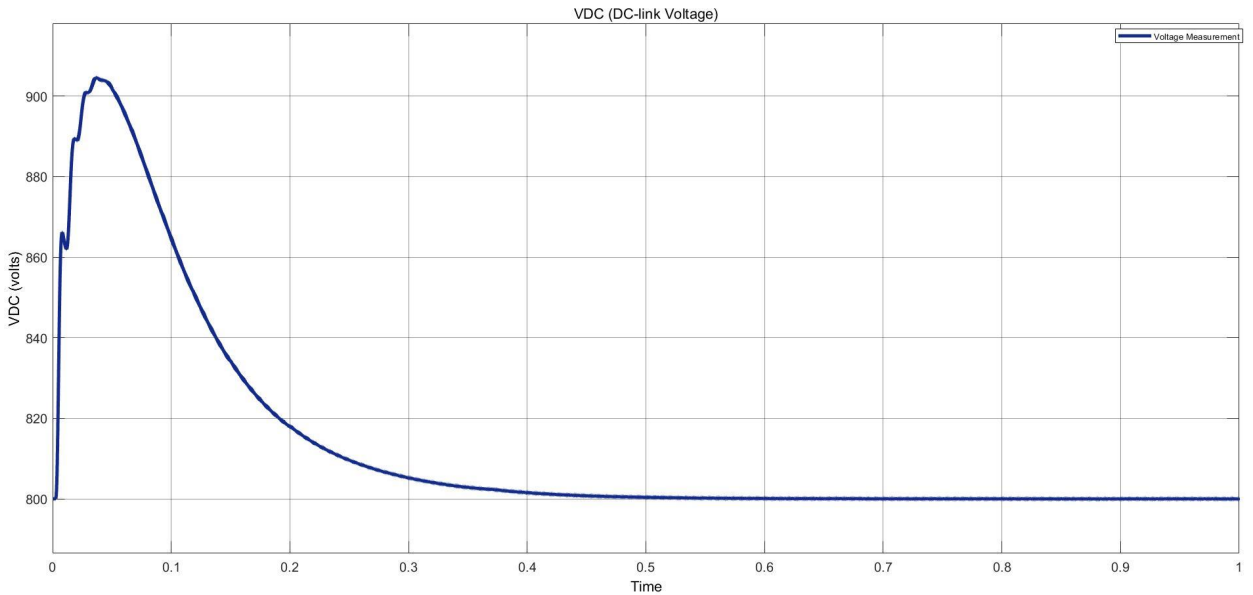


Figure 5.2.2b: DC-link voltage in V2G mode with parallel operation of batteries

5.2.3 G2V WITH PARALLEL OPERATION RESULTS

Figures 5.2.3a and 5.2.3b, below shows the grid three phase voltages-currents waveforms and DC-link voltage respectively in G2V mode with parallel operation of batteries (EVs), the grid voltage and the current waveforms are out-of-phase with each other by an angle of 180^0 which validate the same operation.

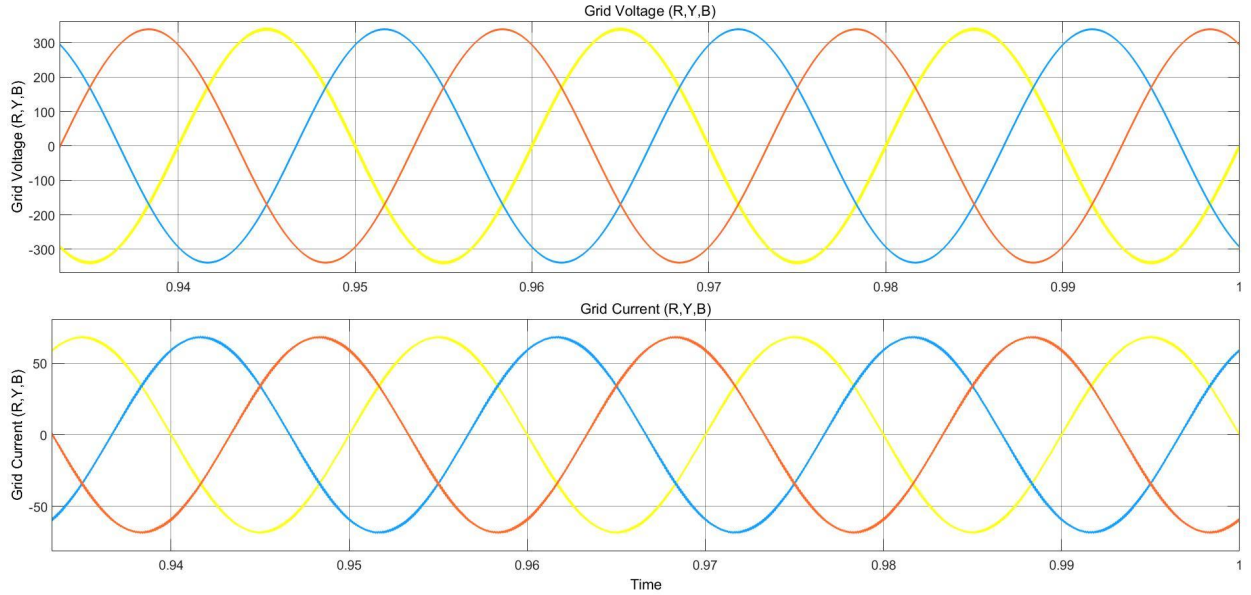


Figure 5.2.3a: Three phase grid voltages and current in G2V mode with parallel operation of batteries

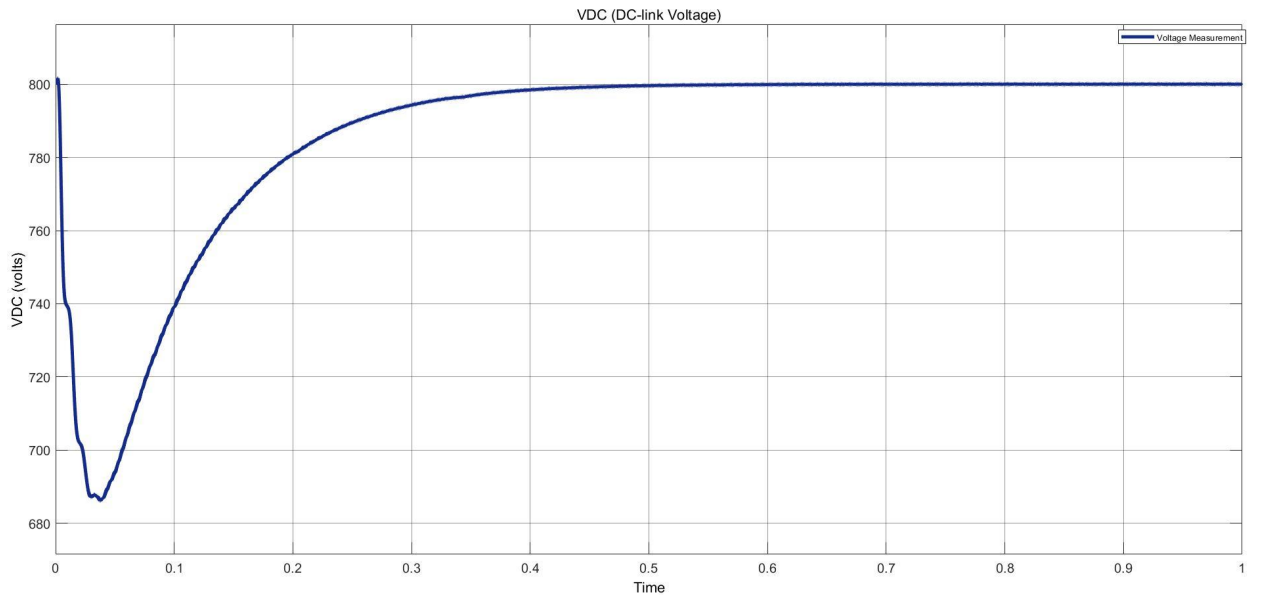


Figure 5.2.3b: DC-link voltage in G2V mode with parallel operation of batteries

5.3 THD COMPARISON

THD (Total Harmonics Distortion) plays an important role in deciding whether the injection of power is suitable for the grid or not. Higher content of THD power injection can leads to injection of unwanted harmonics which is not suitable for the grid's stability and end user applications, so as per IEEE standards %THD less than 5% are considered suitable for power injection for the grid

5.3.1 THD IN SINGLE BATTERY V2G & G2V OPERATION

The total harmonic distortion (%THD) using FFT analysis obtained for the grid current is equal to 2.45% as shown in the below FFT window of MATLAB Fig 5.3.1, which is well below the IEEE standards of 5% (519-1992).

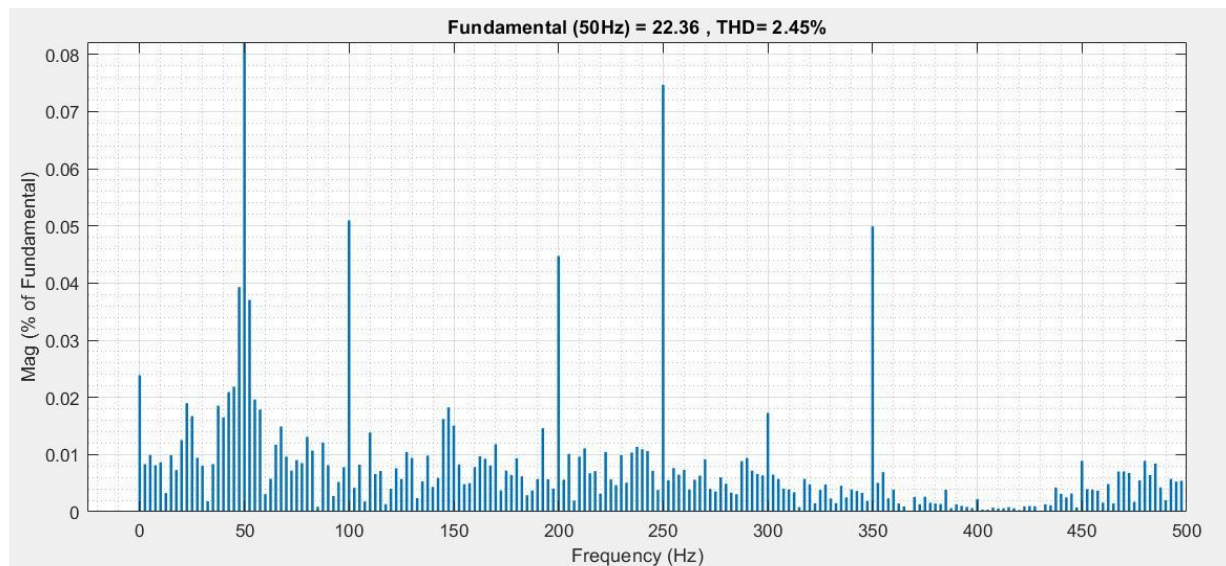


Figure 5.3.1: FFT window of single battery V2G-G2V operation

5.3.2 THD IN PARALLEL OPERATION OF BATTERIES V2G-G2V OPERATION

The %THD obtained for the grid current in parallel operation of batteries is equal to 0.93% as shown in the below FFT window of MATLAB Fig 5..3.2, which is well below the IEEE standards of 5% and which is further improved when compared to above operation of single battery V2G-G2V system.

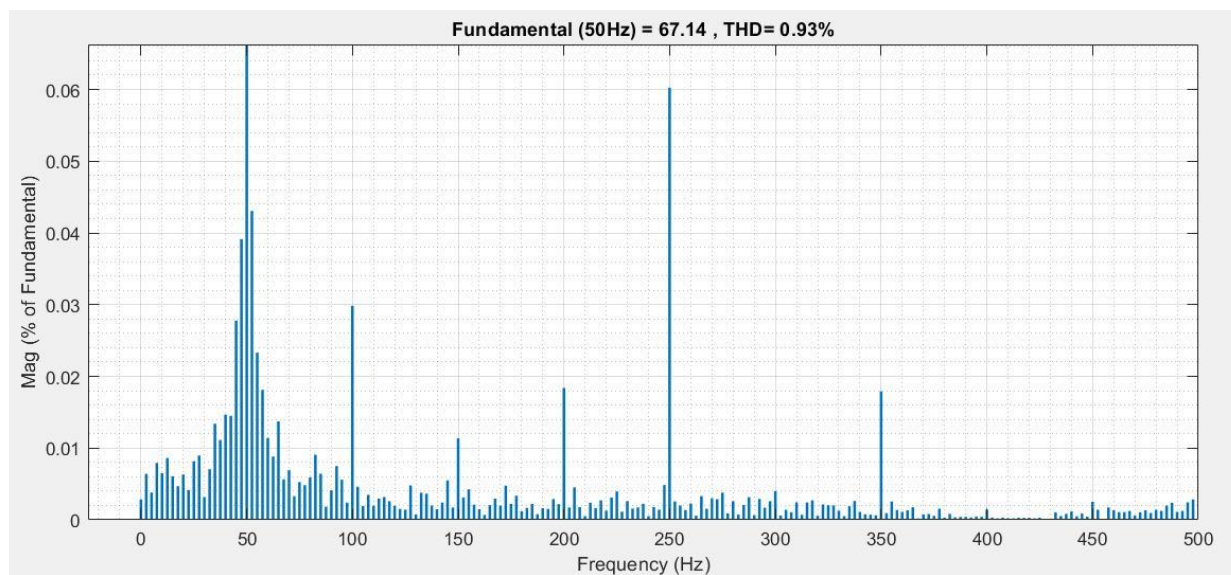


Figure 5.3.2: FFT window of parallel battery V2G-G2V operation

6. CONCLUSION AND POSSIBLE FUTURE WORK

This chapter will provide a detailed technical assessment of harmonics, working, power flow in addition with various topologies (power-electronics) simulated and explained in previous chapters.

6.1 PERFORMANCE RELATED TO OPERATIONS

The performance of V2G and G2V systems at an instance point time with exact values obtained during summation are discussed using table 6.1 below, measured at time = 0.505 sec. This gives a glimpse of performance of the designed system.

Table 6.1: Performance parameters of V2G and G2V mode at t=0.505 sec

Parameters	Operations	
	V2G	G2V
Grid Phase Voltage (Va)	339 Volts	338.974 Volts
Grid Phase Current (Ia)	23.081 Amps	-22.967 Amps
Active Power (P)	11.31 KW	-11.69 KW
Reactive Power (Q)	172 Kvar	-92.53 KVar
DC-Link Voltage (Vdc)	800.1	799.9
Battery Current (Ibat)	30.50	-29.52
Battery Voltage (Vbat)	387.0	388.5
Battery SOC status	Decreases	Increases

6.2 RESULTS

In the complete designing and simulating different topologies for V2G-G2V systems using a PLL controller, the performance parameter in terms harmonic distortion was measure for the grid current which was well below 5%, i.e 2.45% and 0.93% for single and parallel battery (EVs) operation respectively. It was observed that upon increasing the parallel operation can produce a more reliant and efficient system.

6.3 CONCLUSION

In this project various transformer-less topologies for V2G-G2V system and subsystem were designed to operate with a controller in place i.e PLL, that automated the power flow and operating conditions as per the requirements. This system is made more suitable for integration of renewable energy applications. It is concluded that V2G/G2V application can improve the stability, efficiency and reliability of the gird and the traction (EVs) with added auxiliary loads.

The project delivered a technical review for power flow and modeling of various power electronics converter topologies with their control strategies using MATLAB/SIMULINK. The THD (%) obtained were within the standard IEEE limits and which is further reduced with parallel batteries operation.

6.4 FUTURE WORK

This V2G/G2V technology has a major role to play in the upcoming future, as the world is moving more towards renewable energy sources and EVs are playing a predominant role. It is in benefit of future demand to work on technologies which implements V2G/G2V with a standalone inverter system which can be used to feed and cater unbalanced loads and support more auxiliary services with increased efficiency.

Further integration of this kind of system with technologies like cyber physical systems (CPS) can be a game changer in this field, this will provide the user with power to control and monitor the system remotely to act accordingly. Developing monetization policies for users to support grid requirements with the help of renewable energy source integration by the government will boost and support the current renewable-energy ecosystem as a whole.

References

- [1] Z. Zhang, B. Liu and S. Song, "Power Decoupling Control for V2G/G2V/PV2G Operation Modes in Single-Phase PV/Battery Hybrid Energy System With Low DC-Link Capacitance," in IEEE Access, vol. 9, pp. 160975-160986, 2021, doi: 10.1109/ACCESS.2021.3131626.
- [2] M. A. Islam et al., "Modeling and Performance Evaluation of ANFIS Controller-Based Bidirectional Power Management Scheme in Plug-In Electric Vehicles Integrated With Electric Grid," in IEEE Access, vol. 9, pp. 166762-166780, 2021, doi: 10.1109/ACCESS.2021.3135190.
- [3] B. Chelladurai, C. K. Sundarabalan, S. N. Santhanam and J. M. Guerrero, "Interval Type-2 Fuzzy Logic Controlled Shunt Converter Coupled Novel High-Quality Charging Scheme for Electric Vehicles," in IEEE Transactions on Industrial Informatics, vol. 17, no. 9, pp. 6084-6093, Sept. 2021, doi: 10.1109/TII.2020.3024071.
- [4] A. K. Seth and M. Singh, "Second-Order Ripple Minimization in Single-Phase Single-Stage Onboard PEV Charger," in IEEE Transactions on Transportation Electrification, vol. 7, no. 3, pp. 1186-1195, Sept. 2021, doi: 10.1109/TTE.2021.3049559.
- [5] H. -C. Chen and B. -W. Huang, "Integrated G2V/V2G Switched Reluctance Motor Drive With Sensing Only Switch-Bus Current," in IEEE Transactions on Power Electronics, vol. 36, no. 8, pp. 9372-9381, Aug. 2021, doi: 10.1109/TPEL.2021.3054875.
- [6] S. H. Hosseini, R. Ghazi and H. Heydari-Doostabad, "An Extendable Quadratic Bidirectional DC-DC Converter for V2G and G2V Applications," in IEEE Transactions on Industrial Electronics, vol. 68, no. 6, pp. 4859-4869, June 2021, doi: 10.1109/TIE.2020.2992967.
- [7] A. Verma and B. Singh, "AFF-SOGI-DRC Control of Renewable Energy Based Grid Interactive Charging Station for EV With Power Quality Improvement," in IEEE Transactions on Industry Applications, vol. 57, no. 1, pp. 588-597, Jan.-Feb. 2021, doi: 10.1109/TIA.2020.3029547.
- [8] J. -J. Kao, C. -L. Lin, Y. -C. Liu, C. -C. Huang and H. -S. Jian, "Adaptive Bidirectional Inductive Power and Data Transmission System," in IEEE Transactions on Power Electronics, vol. 36, no. 7, pp. 7550-7563, July 2021, doi: 10.1109/TPEL.2020.3047069.
- [9] K. P. Inala, B. Sah, P. Kumar and S. K. Bose, "Impact of V2G Communication on Grid Node Voltage at Charging Station in a Smart Grid Scenario," in IEEE Systems Journal, vol. 15, no. 3, pp. 3749-3758, Sept. 2021, doi: 10.1109/JSYST.2020.3007320.
- [10] G. Guru Kumar and S. Kumaravel, "Dual-Input Non-isolated DC-DC Converter with Vehicle to Grid Feature," in IEEE Journal of Emerging and Selected Topics in Power Electronics, doi: 10.1109/JESTPE.2020.3042967.
- [11] H. Heydari-doostabad and T. O'Donnell, "A Wide-Range High-Voltage-Gain

Bidirectional DC-DC Converter for V2G and G2V Hybrid EV Charger," in IEEE Transactions on Industrial Electronics, vol. 69, no. 5, pp. 4718-4729, May 2022, doi: 10.1109/TIE.2021.3084181.

- [12] K. Sarita et al., "Power Enhancement With Grid Stabilization of Renewable Energy-Based Generation System Using UPQC-FLC-EVA Technique," in IEEE Access, vol. 8, pp. 207443-207464, 2020, doi: 10.1109/ACCESS.2020.3038313.
- [13] H. M. Khalid and J. C. . -H. Peng, "Bidirectional Charging in V2G Systems: An In-Cell Variation Analysis of Vehicle Batteries," in IEEE Systems Journal, vol. 14, no. 3, pp. 3665-3675, Sept. 2020, doi: 10.1109/JST.2019.295896.
- [14] S. Taghizadeh, M. J. Hossain, N. Poursafar, J. Lu and G. Konstantinou, "A Multifunctional Single-Phase EV On-Board Charger With a New V2V Charging Assistance Capability," in IEEE Access, vol. 8, pp. 116812-116823, 2020, doi: 10.1109/ACCESS.2020.3004931.
- [15] S. Liu, D. Xin, L. Yang, J. Li and L. Wang, "A Hierarchical V2G/G2V Energy Management System for Electric-Drive-Reconstructed Onboard Converter," in IEEE Access, vol. 8, pp. 198201-198213, 2020, doi: 10.1109/ACCESS.2020.3034968.
- [16] D. Said and H. T. Mouftah, "A Novel Electric Vehicles Charging/Discharging Management Protocol Based on Queuing Model," in IEEE Transactions on Intelligent Vehicles, vol. 5, no. 1, pp. 100-111, March 2020, doi: 10.1109/TIV.2019.2955370.
- [17] Y. Fu et al., "Design Methodology of a Three-Phase Four-Wire EV Charger Operated at the Autonomous Mode," in IEEE Transactions on Transportation Electrification, vol. 5, no. 4, pp. 1169-1181, Dec. 2019, doi: 10.1109/TTE.2019.2957635.
- [18] C. Viana and P. W. Lehn, "A Drivetrain Integrated DC Fast Charger With Buck and Boost Functionality and Simultaneous Drive/Charge Capability," in IEEE Transactions on Transportation Electrification, vol. 5, no. 4, pp. 903-911, Dec. 2019, doi: 10.1109/TTE.2019.2925211.
- [19] H. Liang, Y. Liu, F. Li and Y. Shen, "Dynamic Economic/Emission Dispatch Including PEVs for Peak Shaving and Valley Filling," in IEEE Transactions on Industrial Electronics, vol. 66, no. 4, pp. 2880-2890, April 2019, doi: 10.1109/TIE.2018.2850030.
- [20] X. Lu and H. Wang, "A Highly Efficient Multifunctional Power Electronic Interface for PEV Hybrid Energy Management Systems," in IEEE Access, vol. 7, pp. 8964-8974, 2019, doi: 10.1109/ACCESS.2018.2889099.
- [21] Y. Hsu, S. Kao, C. Ho, P. Jhou, M. Lu and C. Liaw, "On an Electric Scooter With G2V/V2H/V2G and Energy Harvesting Functions," in IEEE Transactions on Power Electronics, vol. 33, no. 8, pp. 6910-6925, Aug. 2018, doi: 10.1109/TPEL.2017.2758642.
- [22] A. A. S. Mohamed, A. Berzoy, F. G. N. de Almeida and O. Mohammed, "Modeling and Assessment Analysis of Various Compensation Topologies in Bidirectional IWPT System for EV Applications," in IEEE Transactions on Industry Applications, vol. 53, no. 5, pp. 4973-4984, Sept.-Oct. 2017, doi: 10.1109/TIA.2017.2700281.